Luo et al. *Zool. Res.* 2022, 43(5): 787−804
https://doi.org/10.24272/j.issn.2095-8137.2022.081

ZR | Zoological Research

Article Open Access

Phylogenetic analysis of combined mitochondrial genome and 32 nuclear genes provides key insights into molecular systematics and historical biogeography of Asian warty newts of the genus *Paramesotriton* (Caudata: Salamandridae)

Tao Luo[1,2,#], Sha-Sha Yan[2,#], Ning Xiao[3], Jia-Jun Zhou[4], Xing-Liang Wang[2], Wei-Cai Chen[5], Huai-Qing Deng[1,*], Bao-Wei Zhang[6,*], Jiang Zhou[2,*]

[1] *School of Life Sciences*, *Guizhou Normal University*, *Guiyang*, *Guizhou* 550025, *China*
[2] *School of Karst Science*, *Guizhou Normal University*, *Guiyang*, *Guizhou* 550001, *China*
[3] *Guiyang Healthcare Vocational University*, *Guiyang*, *Guizhou* 550081, *China*
[4] *Zhejiang Forest Resource Monitoring Center*, *Hangzhou*, *Zhejiang* 310020, *China*
[5] *Key Laboratory of Environment Change and Resources Use in Beibu Gulf Ministry of Education*, *Nanning Normal University*, *Nanning*, *Guangxi* 530001, *China*
[6] *School of Life Sciences*, *Anhui University*, *Hefei*, *Anhui* 230601, *China*

ABSTRACT

The *Paramesotriton* Chang, 1935 genus of Asian warty newts is the second most diverse genus in the family Salamandridae, currently containing 14 recognized species from northern Vietnam to southwest-central and southern China. Although species of this genus have been included in previous phylogenetic studies, the origin and interspecific relationships of the genus are still not fully resolved, especially at key nodes in the phylogeny. In this study, we sequenced mitochondrial genomes and 32 nuclear genes from 27 samples belonging to 14 species to reconstruct the interspecific phylogenetic relationships within *Paramesotriton* and explore its historical biogeography in southern China. Both Bayesian inference and maximum-likelihood analyses highly supported the monophyly of *Paramesotriton* and its two recognized species groups (*P. caudopunctatus* and *P. chinensis* groups) and further identified five hypothetical phylogenetic cryptic species. Biogeographic analyses indicated that *Paramesotriton* originated in southwestern China (Yunnan-Guizhou Plateau/South China) during the late Oligocene. The time of origin of

Received: 11 May 2022; Accepted: 19 August 2022; Online: 19 August 2022

Foundation items: This study was supported by the Guizhou Province Top Discipline Construction Program Project (Qianjiao Keyan Fa[2019]125), Postgraduate Education Innovation Programme of Guizhou Province (Qianjiaohe YJSKYJJ (2021) 091), Strategic Priority Research Program B of the Chinese Academy of Sciences (CAS) (XDB31000000), National Animal Collection Resource Center, China, and Application of Amphibian Natural Antioxidant Peptides as Cosmetic Raw Material Antioxidants (QKZYD [2020]4002)

[#]Authors contributed equally to this work

*Corresponding authors, E-mail: huaiqingdeng@gznu.edu.cn; zhangbw@ahu.edu.cn; zhoujiang@ioz.ac.cn

Paramesotriton corresponded to the second uplift of the Himalayan/Qinghai-Xizang (Tibetan) Plateau (QTP), rapid lateral extrusion of Indochina, and formation of karst landscapes in southwestern China. Principal component analysis (PCA), independent sample *t*-tests, and niche differentiation using bioclimatic variables based on locations of occurrence suggested that *Paramesotriton* habitat conditions in the three current regions (West, South, and East) differ significantly, with different levels of climatic niche differentiation. Species distribution model (SDM) predictions indicated that the most suitable distribution areas for the *P. caudopunctatus* and *P. chinensis* species groups are western and southern/eastern areas of southern China. This study increases our knowledge of the taxonomy, biodiversity, origin, and suitable distribution areas of the genus *Paramesotriton* based on phylogenetic, biogeographic, and species distribution models.

Keywords: *Paramesotriton*; Systematics; Biogeography; Southern China

INTRODUCTION

Mountain ecosystems often show high species richness and diversity due to a combination of geology and climate (Antonelli et al., 2018; Hazzi et al., 2018; Rahbek et al., 2019a, 2019b). Southern China has long been considered as a little-known and highly threatened biodiversity hotspot and a priority area for biodiversity conservation by the Chinese government (Hu et al., 2021; Ministry of Environmental Protection, 2015; Myers et al., 2000). High diversity and regional endemism provide the opportunity to trace the roles of complex geological and climatic histories in species diversity. In recent years, a number of biogeographic studies have explored the evolutionary history of different ecotypes in southern China, including cave fish (Wen et al., 2022), amphibians and reptiles (Che et al., 2010; Chen et al., 2018a; Guo et al., 2020; Hofmann et al., 2019; Wang et al., 2018a; Xu et al., 2021; Yan et al., 2021), invertebrates (Zhao & Li, 2017), and plants (Xiang et al., 2021; Zhao et al., 2021). However, little is known about the origin and dispersal of salamanders, such as Asian warty newts, in this region.

The *Paramesotriton* Chang, 1935 genus of Asian warty newts is the second most diverse genus within the family Salamandridae, containing 14 recognized species distributed in mountain streams and rivers in southern China and northern Vietnam (AmphibiaChina, 2022; Frost, 2021). Species in *Paramesotriton* are highly dependent on riverine habitats and typically have a narrow distribution due to their low dispersal ability and reliance on water bodies (Fei et al., 2006; Zhao et al., 2012). Thus, species within this genus are ideal for exploring the evolutionary history and drivers of speciation of aquatic fauna. However, populations continue to decline due to habitat loss as a result of environmental pollution, climate change, and anthropogenic disturbance (e.g., dam construction, tourism, pet trade, and agriculture) (IUCN, 2022; Zhao et al., 2012). For example, *P. guangxiensis*, *P. zhijinensis*, and *P. yunwuensis* are considered endangered (IUCN, 2022), with wild populations currently threatened with extinction and requiring conservation attention. Short-term evolutionary histories of species (e.g., recent species formation and adaptive radiation) exhibiting high morphological similarity can mislead assessment of species diversity and evolutionary relationships, leading to poor conservation decisions. Therefore, molecular analyses are required to elucidate the species diversity, evolutionary relationships, and conservation units in *Paramesotriton* (Luo et al., 2021).

Unstable and uncertain phylogenetic relationships may affect our understanding of diversity and evolutionary history. The phylogenetic position of *Paramesotriton* within the family Salamandridae has been resolved (Kieren et al., 2018; Zhang et al., 2008), but relationships within *Paramesotriton* remain poorly understood, especially between species groups (Dubois & Raffaëlli, 2009; Dubois et al., 2021; Fei et al., 2006; Fei & Ye, 2016; Gu et al., 2012a; Yuan et al., 2014; Supplementary Figure S1 and Table S1). Fei et al. (2006) divided Chinese *Paramesotriton* species into the *P. caudopunctatus* and *P. chinensis* species groups based on morphological characters, which were accepted by later researchers (Gu et al., 2012a, 2012b; Wang et al., 2013; Wu et al., 2010; Yuan et al., 2014, 2016a; Zhao et al., 2008). Subsequently, Fei & Ye (2016) divided Chinese *Paramesotriton* species into the three subgenera *Allomesotriton*, *Karstotriton*, and *Paramesotriton* based on skeletal and morphological characters (Supplementary Table S1). Several recent phylogenetic studies have attempted but failed to resolve the relationship between the two species groups (Gu et al., 2012a; Yuan et al., 2014, 2016a). Furthermore, current taxonomic hypotheses regarding the relationships within and between the two species groups (or three subgenera) depend on morphological characters and single fragments of mitochondrial DNA (mtDNA) sequences. Therefore, expanded sample collection and additional molecular markers are required for phylogenetic analysis to resolve the interspecific relationships and evolutionary history of *Paramesotriton*.

Herein, based on the most complete and expanded sampling to date, the phylogeny and biogeography of the genus *Paramesotriton* was inferred using mitochondrial and nuclear locus data, with results used to analyze environmental variables based on occurrence data. The study objectives were to (1) explore the interspecific relationships of the genus *Paramesotriton*, and (2) identify the center of origin, estimate dates of each divergence event, and reconstruct the evolutionary history of the genus.

MATERIALS AND METHODS

Taxon sampling and sequence collection

A total of 23 *Paramesotriton* samples were collected from Guizhou, Zhejiang, Guangxi, Guangdong, Hubei, Yunnan, Jiangxi, and Hong Kong, China (Figure 1), representing 14 recognized species and putative cryptic species. We also searched the National Center for Biotechnology Information

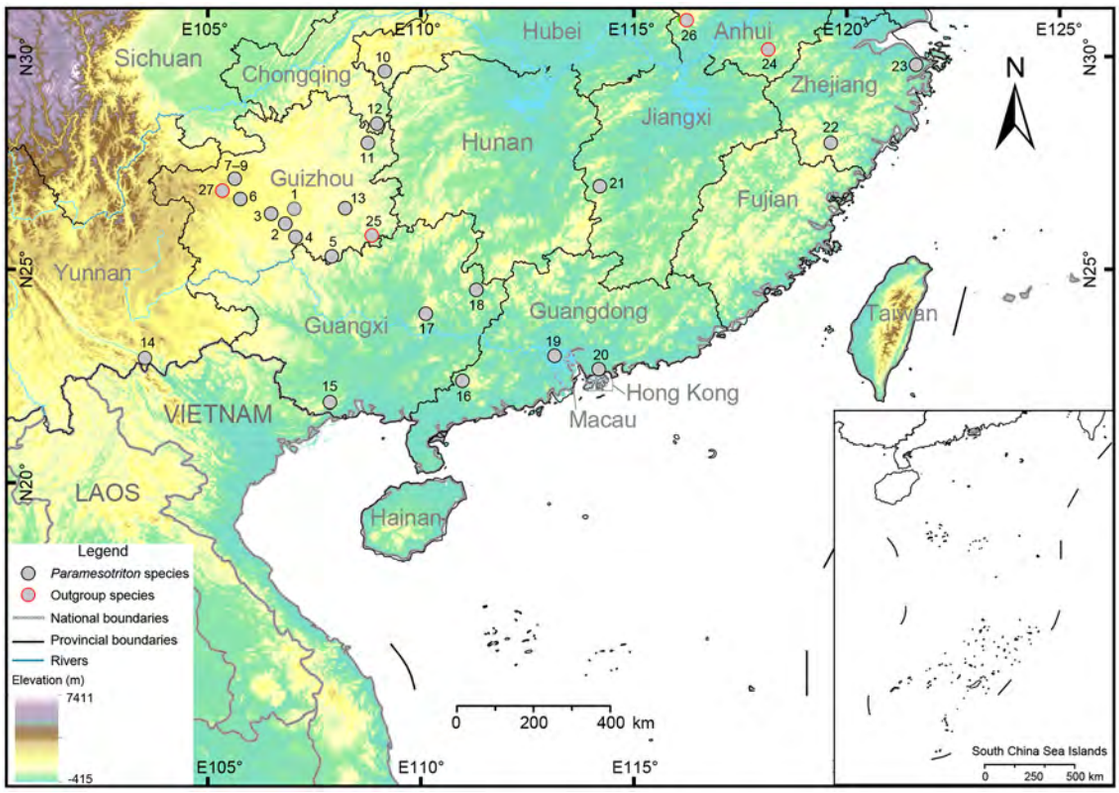

Figure 1 Locations of 14 species of *Paramesotriton* and four outgroup samples collected for this study
Numbers correspond to ID numbers in Supplementary Table S3.

(NCBI, https://www.ncbi.nlm.nih.gov/) database using "*Paramesotriton* mitochondrion, complete genome" as keywords (as of 7 January 2022) and downloaded the mitochondrial genome (mitogenome) of the genus for phylogenetic analysis (see Supplementary Table S2 for more details). Following Zhang et al. (2008), we selected *Pachytriton feii*, *Pachytriton inexpectatus*, *Cynops orientalis*, *Tylototriton kweichowensis*, and *Tylototriton asperrimus* as outgroups for phylogenetic analysis. Species names, localities, specimen vouchers, and accession numbers of outgroups and ingroups are provided in Supplementary Table S2. All samples for molecular analysis are kept at the Guizhou Normal University, Guiyang City, Guizhou Province, China.

DNA extraction, amplification, and sequencing

Genomic DNA for each sample was extracted from 95% ethanol-preserved tissue using the cetyltrimethylammonium bromide (CTAB) method (Allen et al., 2006). For each sample, DNA was cleaved into small fragments (350 bp) using ultrasound. The end DNA fragments were repaired using 3'-5' nucleic acid exonuclease and polymerase; a single base "A" was added at the 3' end, and sequencing connectors were ligated. The DNA fragments were then selected by agarose gel electrophoresis and polymerase chain reaction (PCR) amplification was performed to form a sequencing library. Sequencing was performed on an Illumina NovaSeq 6000 sequencer. At the end of sequencing, high-quality clean reads were obtained using SOAPnuke v1.3 (Chen et al., 2018b) by the removal of reads with more than 5% N base content, low-quality (≤5) bases up to 50%, and adapters. Ultimately, each sample generated reads that were 150 bp in length and ~4.2 Gb in size. The reads were assembled into mitogenomes using SPAdes v3.14.0 (Bankevich et al., 2012). Assembled contigs were BLAST aligned with the relevant reference genome (*P. caudopunctatus*; EU880326) to identify potential assembly errors. Finally, the included genes in the assembled mitogenomes were annotated using MITOS v2.0 (Bernt et al., 2013).

To obtain a stable phylogenetic framework and resolve interspecific relationships, we also amplified 32 nuclear gene fragments for inclusion in the phylogenetic analysis. All samples were amplified using PCR under the following conditions: initial denaturation step at 98 °C for 3 min; 36 cycles of denaturation at 95 °C for 30 s, annealing at 51–59 °C for 40 s, extension at 72 °C for 1 min, and a final extension at 72 °C for 10 min. PCR primers and detailed annealing temperatures for the 32 nuclear gene fragments are provided in Supplementary Table S3. The purified PCR products were directly sequenced in both directions using an ABI Prism 3730 automated DNA sequencer from TSINGKE Biotechnology Co., Ltd. (Chengdu, China). All newly obtained mitogenomic and nuclear gene sequences were deposited in GenBank under accession Nos. MW524141–MW524143, ON357921–ON357943, ON364656–ON365439, and ON422325 (Supplementary Table S2).

Phylogenetic analysis

The newly obtained mitogenome and nuclear gene sequences

were edited using PhyloSuite v1.2.2 (Zhang et al., 2020) and DNAStar (DNASTAR, Inc., USA). Sequence alignment was performed using MAFFT v7.4 (Katoh & Standley, 2013) with default settings in PhyloSuite v1.2.2. The resulting sequences were checked, and ambiguous alignments were trimmed by eye using MEGA v7.0 (Kumar et al., 2016). For the mitogenome, we selected 39 gene fragments for phylogenetic analysis, i.e., two ribosomal genes (12S, 16S), 13 mitochondrial protein-coding genes (*ATP6*, *ATP8*, *COI*, *COII*, *COIII*, *ND1*, *ND2*, *ND3*, *ND4*, *ND4L*, *ND5*, *ND6*, and cyt *b*), and 24 transfer RNAs (tRNAs). The sequence matrix used for phylogenetic analysis consisted of concatenated mitochondrial data and 32 nuclear loci data. The best-fit partitioning scheme and corresponding nucleotide substitution models for concatenated nucleotides were selected using PartitionFinder v2.1.1 (Lanfear et al., 2017) based on Bayesian information criterion (BIC).

Phylogenetic analysis of concatenated nucleotide sequences was performed under the best-fit partitioning schemes and nucleotide substitution models using Bayesian inference (BI) and maximum-likelihood (ML) in MrBayes v3.2.1 (Ronquist et al., 2012) and IQ-tree v2.0.4 (Nguyen et al., 2015), respectively. ML analysis was run using the best-fit model for each partition with 2 000 ultrafast bootstrap (UFB) replicates (Minh et al., 2013) and was performed until a correlation coefficient of at least 0.99 was reached (Hoang et al., 2018). BI analysis was run independently using four Markov Chain Monte Carlo (MCMC) chains (three heated chains and one cold chain) starting with a random tree; each chain was run for 2×10^7 generations and sampled every 1 000 generations. Convergence of data runs was estimated using average standard deviation of split frequencies (ASDSF) <0.01 and Tracer v1.7.1 (Rambaut et al., 2018) to check for effective sample size (ESS) >200. The phylogenetic tree nodes were considered well-supported when the Bayesian posterior probability (BPP) of the node was ≥0.95 and ML UFB was ≥95%. Using MEGA v7.0 (Kumar et al., 2016), the uncorrected *P*-distance model (1 000 replicates) was used to calculate the average genetic distance between mitogenomes of species.

Divergence-time estimation

We used BEAST v2.6.6 (Bouckaert et al., 2014) to estimate the date of origin of the genus *Paramesotriton* and time of divergence of each species using concatenated nucleotide data under a relaxed clock log-normal assumption and an *a priori* Yule model. In this analysis, three calibration point constraints were used: (1) divergence between primitive newts (*Tylototriton*) and modern Asian newts (*Cynops*, *Paramesotriton*, and *Pachytriton*) dated to 74.2 million years ago (Ma) (Zhang et al., 2008), with a normal prior (mean 74.2; sigma 5.0; offset 0.0); (2) origin of modern Asian newts calibrated to 15 Ma based on nearly complete early Miocene fossils of *Procynops miocenicus*, which are clearly related to *Cynops*, with a log-normal prior (mean 10; sigma 1.0; offset 15) and calibration set to monophyly (Estes, 1981; Kieren et al., 2018); and (3) divergence between the *P. caudopunctatus* group and *P. chinensis* group of the genus *Paramesotriton* dated to 23.8 Ma (95% HPD: 22.4–35.0 Ma; Zhang et al., 2008), with a normal prior (mean 23.8; sigma 2.0; offset 0.0).

BEAST analysis was conducted for a total of 2×10^7 generations, with sampling every 2 000 generations. We used Tracer v1.7.1 (Rambaut et al., 2018) to check the convergence and stability of run parameters, i.e., ESS of parameters >200. Maximum clade credibility (MCC) trees were generated using TreeAnnotator v2.4.1 (Rambaut & Drummond, 2010) by applying a burn-in (as trees) of 10%, posterior probability limit of 0.5, and median height for node selection. Time tree editing and visualization were performed in FigTree v1.4.3 (Rambaut, 2016).

Ancestral area reconstruction

To estimate the origin and dispersal history of *Paramesotriton*, BioGeoBEARS (Matzke, 2013) in RASP v3.2 (Yu et al., 2015) was used to reconstruct ancestral areas and infer their biogeographic history. A time-calibrated phylogenetic tree generated from BEAST analysis was used as the input tree with all outgroups removed, retaining only *Paramesotriton* species. Based on the natural landscape, zoogeography proposed by Zhang (2011), and current distribution of *Paramesotriton*, we used three distribution areas: i.e., (A) Yunnan-Guizhou Plateau; (B) South China/North Vietnam; and (C) East China. Considering the environmental dependence of *Paramesotriton* species, we assumed that extant species would not occur in more than two distribution areas. Therefore, the maximum number of species range areas was limited to two.

Ecological niche modeling, differentiation, and environmental variation analysis

In this study, published and web-recorded data were collected between 2000 and 2021 via multiple means (Supplementary Table S4). If distribution information was only available for location, OvitalMap v9.3.4 was used to infer the coordinates of the location centroid. Records with obvious geocoding errors or where relative accuracy could not be determined were discarded, and duplicate records were manually removed. We use ENMTools v1.3 (Warren et al., 2010) to filter occurrence data based on environmental variable layers to avoid overfitting of prediction results. We collected a total of 165 recorded sites for species in the genus *Paramesotriton*, including 70 recorded sites in the *P. caudopunctatus* species group and 95 recorded sites in the *P. chinensis* species group (East 44, South 51).

Species distribution models (SDMs) for both species groups were predicted using the maximum entropy model implemented in Maxent v3.3.1 (Phillips et al., 2006). The 19 bioclimatic variables (Supplementary Table S5) (resolution 2.5 arc-min) were downloaded from the WorldClim database as environmental data (http://www.worldclim.org, Hijmans et al., 2005a). In SDM analysis, high multicollinearity among bioclimatic variables (Peterson & Nakazawa, 2008), regularization multipliers, and feature classes (Low et al., 2021) were the main factors affecting the prediction results (Radosavljevic & Anderson, 2014). We use two methods to reduce this impact. First, because high multicollinearity between bioclimatic variables may improve SDM accuracy, we used correlation analysis (Pearson's r>0.85; Dormann et al.,

2013) in ENMTools (Warren et al., 2010) to minimize correlation between variables. Second, different regularization multipliers (0.2, 0.4, 0.6, 0.8, 1.0, 1.2, 1.4, 1.6, 1.8, and 2.0) and feature classes were assessed in R using the "kuenm" package (Cobos et al., 2019) to obtain the best combination of runs in Maxent (Phillips et al., 2006; Phillips & Dudík, 2008). Candidate model performance was evaluated based on significance (partial receiver operating curve (ROC), 500 iterations, and 50% of data for bootstraps), omission rate (E=5%), and model complexity (AICc). The best models were selected using on the following criteria: (1) significant model, (2) omission rate ≤5%, and (3) final model delta AICc ≤2 based on best set of models obtained from (1) and (2) (Cobos et al., 2019). As a result, low multicollinearity (Supplementary Figure S2) Bio1 (Annual Mean Temperature), Bio4 (Temperature Seasonality), Bio6 (Min Temperature of Coldest Month), Bio13 (Precipitation of Wettest Month), Bio17 (Precipitation of Driest Quarter), Bio19 (Precipitation of Coldest Quarter), regularization multiplier 1.2 (*P. caudopunctatus* species group)/0.2 (*P. chinensis* species group East or South), and feature class selected linear-quadratic features (*P. caudopunctatus* and *P. chinensis* species groups South/East) were used for SDM analysis (Supplementary Table S6).

Based on the best parameters and models (Supplementary Table S7), to reduce uncertainty caused by sampling artifacts, we randomly divided the distribution data into training data (75%) and validation data (25%) in Maxent. To evaluate the robustness of the models, subsampling was repeated 10 times and the distribution points were repeatedly split into random training and testing subsets, after which the results were averaged. The maximum number of background points and iterations were set to 10 000 and 5 000, respectively, to find the optimal solution, with default values used for the remaining parameters (Hazzi et al., 2018; Morales et al., 2017; Phillips et al., 2006; Radosavljevic & Anderson, 2014). The generated suitability maps were in ASCII format and were visualized using ArcMap v10.4 (Esri). At the same time, we reclassified the suitability layers into four classes based on the predicted results: i.e., unsuitable habitat (0.00–0.25), minimally suitable habitat (0.25–0.50), moderately suitable habitat (0.50–0.75), and highly suitable habitat (>0.75). To explore the key climatic variables that shape the distribution of each species, jackknife tests were performed and response curves for each bioclimatic variable were plotted. To verify the accuracy of each model, we used area under the curve (AUC) (Allouche et al., 2006; Swets, 1988) of the ROC (Hanley & McNeil, 1982) based on following criteria: poor (AUC<0.8), good (AUC 0.90–0.95), and excellent (AUC>0.95) (Guisan & Thuiller, 2005).

Ecological niche overlap of species within the two *Paramesotriton* species groups was measured using occurrence site and spatial environmental data (Broennimann et al., 2012). Climatic niche equivalency among and within species groups (for *P. chinensis* species group) in *Paramesotriton* was estimated based on *I* (Warren et al., 2008) and *D* statistics (Schoener, 1968). Analysis was performed using "ecospat" in the R package with the "niche.equivalency.test" function (Di Cola et al., 2017). Observed values of *D* and *I* were compared to 100 pseudoreplicates, with both statistics ranging from 0 to 1 (Warren et al., 2008). The observed values of *D* and *I* were significantly lower than the niche similarity distribution of 100 replicates and were significantly different (P<0.05), indicating niche differentiation (Warren et al., 2008). In addition, to test whether the ecological niches obtained for the two *Paramesotriton* species groups were identical, climatic niche similarity analysis was conducted using the "ecospat.niche.similarity.test" function in the "ecospat" package in R, i.e., comparing actual occurrence of one species group with random background occurrence of another species group. Here, for niche equivalency and similarity analyses, 100 replicate niche equivalency and background tests were conducted.

Point-based analysis was used to test for differences in bioclimatic variables of the habitats of species from the two species groups in the West, South, and East regions of southern China. Values of the 19 bioclimatic variables for 165 occurrence locations were extracted using DIVAGIS v7.5 (Hijmans et al., 2005b). Principal component analysis (PCA) and independent sample *t*-tests (1 000 bootstrap replicates) were used to test whether differences in ecological niches between the West, South, and East regions were statistically significant.

RESULTS

Nucleotide sequence information

In this study, 27 mitogenomes and 784 sequences from 32 nuclear loci were obtained by sequencing (including outgroups) (Supplementary Table S2). We downloaded seven mitogenomes and 30 nuclear gene sequences from GenBank (Supplementary Table S2). The combined mtDNA (15 408 bp) included 5 774 variable sites and 4 623 parsimony-informative sites. Alignment of concatenated nuclear DNA (nuDNA) contained a total of 27 023 bp, including 1 827 variable sites and 1 150 parsimony-informative sites. Finally, we obtained a matrix of concatenated mtDNA and nuDNA sequences with a total length of 42 431 bp. Detailed information of each sequence dataset and best-fit nucleotide substitution model for each partition are listed in Supplementary Table S8.

Phylogenetic inference

The phylogenetic trees obtained from the concatenated mtDNA and nuDNA datasets using BI and ML analyses showed similar topologies (Figure 2). Both BI and ML analyses highly supported the monophyly of *Paramesotriton* and the monophyly of the *P. caudopunctatus* (Clade A) and *P. chinensis* species groups (Clade B) (BPP=1.00; UBP=100%). The *P. caudopunctatus* species group consisted of five species, i.e., *P. caudopunctatus*, *P. wulingensis*, *P. zhijinensis*, *P. maolanensis*, and four populations of *P. longliensis* (Longli, Huishui, Dafang, and Hubei populations) and could be further divided into two subclades. Subclade A1 consisted of *P. caudopunctatus* and *P. wulingensis*, and subclade A2 consisted of *P. zhijinensis*, *P. maolanensis*, and *P. longliensis*. The *P. chinensis* species group consisted of nine species, i.e., *P. fuzhongensis*, *P. yunwuensis*, *P.*

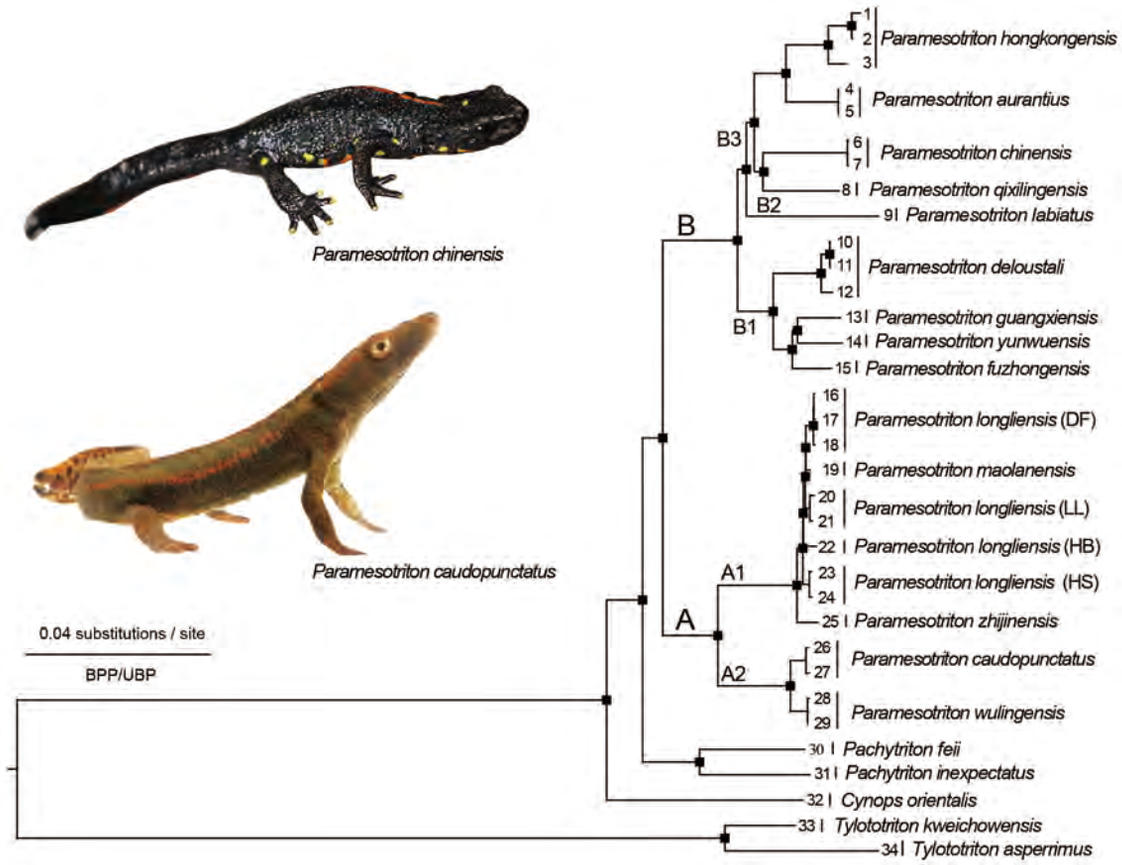

Figure 2 Phylogenetic tree reconstructed using BI and ML methods based on concatenated mtDNA and nuDNA datasets for the genus *Paramesotriton* and outgroups

Black squares at nodes indicate BPP>0.95 for BI analysis and UBP>95 for ML analysis. Numbers at tip of branches correspond to ID numbers in Supplementary Table S9. DF, LL, HS, and HB denote collection from Dafang County, Longli County, Huishui County (Guizhou Province, China), and Xianfeng County (Hubei Province, China), respectively. Species photos from top to bottom denote type species of *P. caudopunctatus* and *P. chinensis* species groups. Photos by Jia-Jun Zhou (*Paramesotriton chinensis*) and Tao Luo (*Paramesotriton caudopunctatus*).

guangxiensis, *P. deloustali*, *P. labiatus*, *P. qixilingensis*, *P. chinensis*, *P. aurantius*, and *P. hongkongensis*, and could be further divided into three subclades. Subclade B1 consisted of *P. fuzhongensis*, *P. yunwuensis*, *P. guangxiensis*, and two populations of *P. deloustali*. Subclade B2 consisted of *P. labiatus* and subclade B3 consisted of *P. qixilingensis*, *P. chinensis*, *P. aurantius*, and two populations of *P. hongkongensis*.

The average mtDNA-based uncorrected *P*-distances between and within species of *Paramesotriton* are provided in Table 1, with interspecific genetic distances ranging from 0.52% (*P. maolanensis* vs. *P. longliensis* (LL)) to 11.84% (*P. zhijinensis* vs. *P. labiatus*). Within subclade A1 of the *P. caudopunctatus* species group, average *P*-distances ranged from 0.52% to 1.83%, with average *P*-distances of 2.19% and 1.05% within the *P. hongkongensis* and *P. deloustali* populations, respectively (Table 1).

Spatiotemporal analysis based on concatenated mtDNA and nuDNA data

The time tree generated from the BEAST run was consistent with the phylogenetic trees inferred by BI and ML, except for subclade A. Spatiotemporal maps of divergence time and ancestral area reconstructions are shown in Figure 3. The date of the stem node of *Paramesotriton* was estimated at 25.42 Ma (95% highest posterior density (HPD): 21.27–29.79 Ma). The time to the most recent common ancestor of the genus *Paramesotriton* and the split between the *P. caudopunctatus* and *P. chinensis* species groups was estimated at 22.86 Ma (node 1; 95% HPD: 19.38–26.45 Ma) (Figure 3B). Early lineage diversification of *Paramesotriton* occurred in the mid-Miocene (15.69–10.19 Ma; nodes 2–6). Lineage diversification of the *P. caudopunctatus* and *P. chinensis* species groups occurred in the mid- to late Miocene (15.69–5.94 Ma) and Pliocene/Pleistocene boundary (3.06–1.28 Ma).

Comparisons of the six models within BioGeoBEARS using corrected Akaike information criterion (AICc) weighting are listed in Table 2. Results showed that the fit of the two remaining " +J" models, but not the DEC+J model, was significantly better compared to the models without " +J ", indicating the importance of founder event speciation in explaining biogeographic patterns (Table 2). According to the best-fit model DIVALIKE+J (Figure 3B), both vicariance and dispersal events may have acted as the main driving forces

Table 1 Uncorrected mean *P*-distances (%) between *Paramesotriton* species on mitogenome

ID	Species	1	2	3	4	5	6	7	8	9	10	11	12	13	14	15	16	17	18
1	*P. wulingensis*																		
2	*P. caudopunctatus*	1.73																	
3	*P. zhijinensis*	7.78	7.75																
4	*P. longliensis* (LL)	7.60	7.54	1.71															
5	*P. longliensis* (HS)	7.53	7.50	1.69	0.74														
6	*P. longliensis* (DF)	7.56	7.52	1.74	0.59	0.78													
7	*P. longliensis* (HB)	7.66	7.63	1.83	0.95	0.93	0.98												
8	*P. maolanensis*	7.52	7.46	1.66	0.52	0.72	0.55	0.92											
9	*P. fuzhongensis*	10.41	10.31	10.87	10.74	10.74	10.76	10.78	10.68										
10	*P. yunwuensis*	10.77	10.68	11.17	11.04	11.01	11.09	11.10	10.98	3.90									
11	*P. guangxiensis*	10.76	10.69	10.95	10.82	10.81	10.85	10.92	10.76	4.03	4.04								
12	*P. deloustali* (Yunnan)	10.22	10.09	10.78	10.67	10.65	10.68	10.73	10.59	5.05	5.42	5.25							
13	*P. deloustali* (VN)	10.21	10.07	10.70	10.59	10.58	10.59	10.64	10.49	5.14	5.34	5.27	1.05						
14	*P. labiatus*	11.33	11.30	11.84	11.64	11.61	11.62	11.74	11.63	8.64	8.87	8.61	8.50	8.58					
15	*P. qixilingensis*	10.54	10.55	10.80	10.76	10.78	10.76	10.77	10.68	7.21	7.52	7.45	7.29	7.25	8.49				
16	*P. chinensis*	10.69	10.59	11.06	10.91	10.91	10.97	11.00	10.87	7.62	7.70	7.71	7.35	7.38	8.59	6.74			
17	*P. aurantius*	10.35	10.37	10.90	10.69	10.67	10.65	10.75	10.63	7.68	7.76	7.83	7.44	7.39	8.39	6.84	7.03		
18	*P. hongkongensis* (GD)	10.93	10.79	11.32	11.06	11.04	11.07	11.14	11.07	8.03	8.08	8.20	7.86	7.88	9.05	7.48	7.92	5.49	
19	*P. hongkongensis* (HK)	10.65	10.56	11.11	10.94	10.91	10.94	11.01	10.91	7.75	7.81	7.82	7.56	7.59	8.66	7.19	7.39	5.02	2.19

DF, LL, HS and HB denote abbreviations collected from Dafang County, Longli County, Huishui County, Guizhou Province, China and Xianfeng County, Hubei Province, China. VN denote abbreviations collected from Vietnam.

shaping the current geographic distribution patterns of the genus *Paramesotriton*.

The BioGeoBEARS results for the best model (DIVALIKE+J) suggested that the recent ancestor of extant species of the genus *Paramesotriton* was most likely distributed on the Yunnan-Guizhou Plateau/South China and dispersed into Guizhou in South China after a vicariance event (Figure 3B; node 1). The *P. caudopunctatus* species group originated from the Yunnan-Guizhou Plateau (mainly Guizhou), and the *P. chinensis* species group originated from southern China. At least four dispersal events and two vicariance events occurred in the mid-Miocene (12.81–8.65 Ma; nodes 6–7). During the mid-Miocene (12.81 Ma; node 6), dispersal events from southern to eastern China initiated the formation and expansion of subclade B3 (Figure 2). During the Miocene (8.65 Ma; node 7), a dispersal event from eastern to southern China (Hong Kong and Guangdong, China) was the origin of the formation of *P. hongkongensis*. Finally, the current geographic distribution patterns within the *P. caudopunctatus* and *P. chinensis* species groups were formed by 13 and 12 speciation events, respectively.

Suitable distribution, climatic niche differentiation, and environmental variation analysis

The SDMs generated good predictions of occurrence locations under current climate scenarios. The AUCs for the *P. caudopunctatus* species group (West), *P. chinensis* species group (East), and *P. chinensis* species group (South) across the observation region were 0.988, 0.987, and 0.991, respectively. The most suitable habitats for the *P. caudopunctatus* species group (West) were in the karst mountain ecosystems of Guizhou in southwestern China, and moderately suitable habitats were located in the Wuling Mountains (southeastern Chongqing, northwestern Hunan, and western Hubei) (Figure 4A). In the East, suitable habitats for the *P. chinensis* species group (East) were found in Fujian, Zhejiang, Jiangxi, and Anhui in eastern China and in the Nanling Mountains (southern Hunan, and southern Jiangxi) and Luoxiao Mountains (Figure 4B). In the South, suitable habitats for the *P. chinensis* species group (South) were found in Guangdong, Hong Kong, southern Guangxi, and southern Fujian (Figure 4C).

Species within the two *Paramesotriton* species groups exhibited different levels of niche differentiation (Figure 5). Climatic niche equivalency analysis indicated that both *I* and *D* values (<0.1) were close to 0 (Figure 5A–F), suggesting that the niches between the *P. caudopunctatus* (West) and *P. chinensis* species groups (East), *P. caudopunctatus* (West) and *P. chinensis* species groups (South), and *P. chinensis* (East) and *P. chinensis* species groups (South) were close to non-overlapping (Figure 5M–P). Niche similarity tests showed that the null hypothesis of identical niche occupation was rejected between the *P. chinensis* (East), *P. chinensis* (South), and *P. caudopunctatus* species groups (West), suggesting that the pairs occupied different niches, although this was not strongly supported ($P>0.05$, Figure 5G, H, K, L). The spatial similarity of occupied niches between the *P. caudopunctatus* (West) and *P. chinensis* species groups (East) was more similar than the simulated random distribution but was not significantly supported ($P>0.05$, Figure 5I, J).

PCA of the 19 bioclimatic variables generated four principal components (PC1=56.39%, PC2=24.41%, PC3=11.18%, and PC4=5.57%), which explained 96.55% of total variance in ecological niche differences under the current climate scenario (Table 3). The PC1 and PC2 scatter plots are shown in Figure 4D, which clearly separated the *P. caudopunctatus*

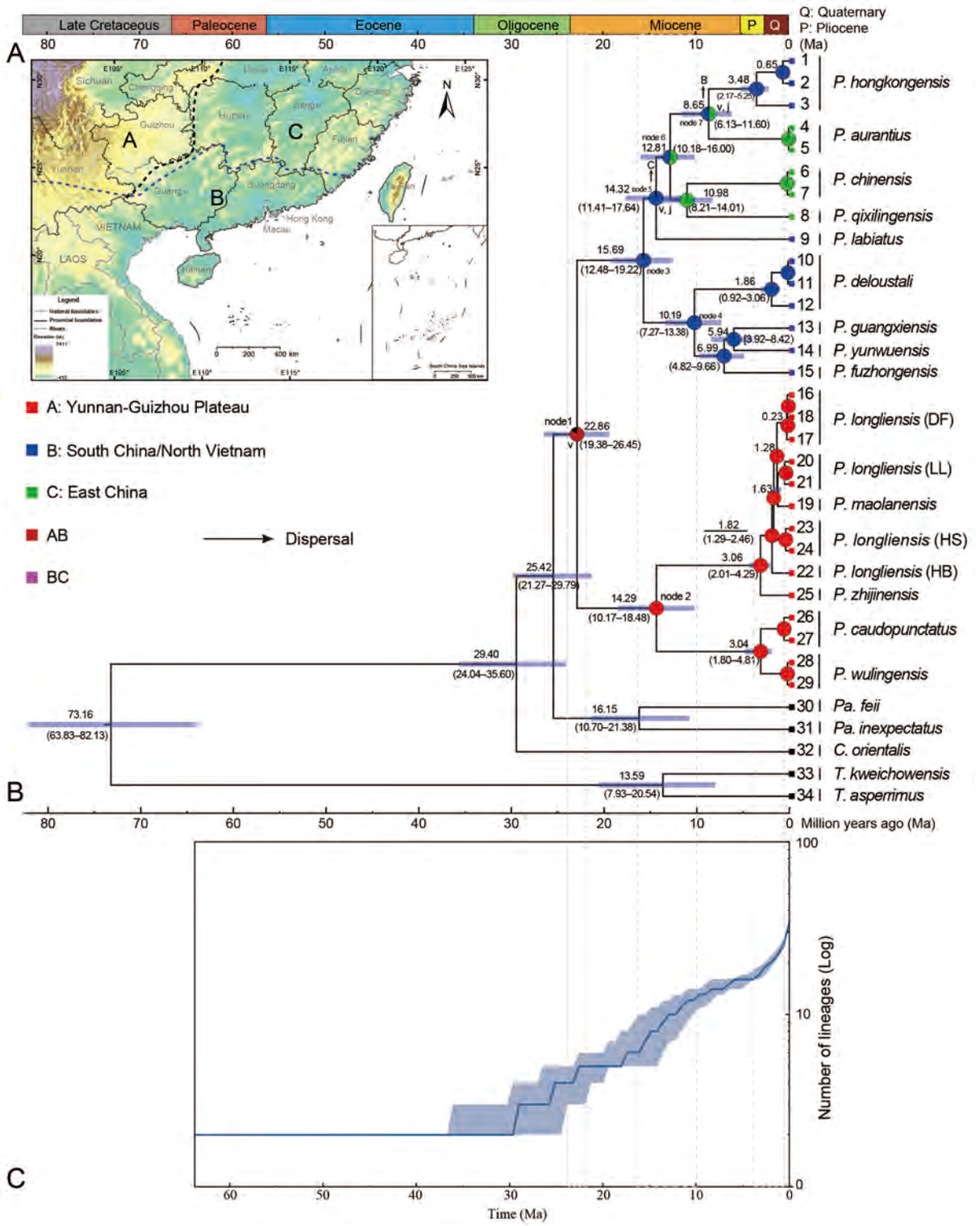

Figure 3 Distribution areas (A) and time-calibrated topology of the genus *Paramesotriton*, reconstructed ancestral area of *Paramesotriton* based on best-fit model (DIVALIKE+J) using BioGeoBEARS (B), and lineage-through-time (LTT, logarithmic scale) plot (C) Divergence times were estimated with BEAST using concatenated mtDNA and nuDNA data. Numbers at nodes represent mean node ages. Blue bar at each node indicates 95% credibility intervals, with exact values in brackets. Color-coded boxes reflect biogeographic designations (for species at tips) and most probable states at each node. v, vicariance; j, jump-dispersal or founder-event speciation. For LTT plots, all trees were pruned from final topology-constrained BEAST analysis, and the maximum credibility tree is denoted by a thick sky-blue line. Numbers at tip of branches correspond to ID numbers in Supplementary Table S9.

Table 2 BioGeoBEARS estimations of ancestral areas based on phylogeny of the genus *Paramesotriton*

Model	LnL	Number of parameters	Parameters			AICc	AICc model weight
			d	e	j		
DEC	−11.34	2	0.0033	1E-12	0	27.15	0.3
DEC+J	−11.34	3	0.0033	1E-12	0.00001	29.65	0.085
DIVALIKE	−11.76	2	0.0062	1E-12	0	27.98	0.19
DIVALIKE+J	**−9.81**	**3**	**1E-12**	**1E-12**	**0.021**	**26.58**	**0.39**
BAYAREALIKE	−18.52	2	0.0059	0.033	0	41.5	0.0002
BAYAREALIKE+J	−12.26	3	0.0000001	0.0000001	0.03	31.48	0.034

Six models were tested and compared using corrected Akaike Information Criterion (AICc) weighting. Best model is highlighted in bold. LnL: Log-likelihood; d: Dispersal rate per million years along branches; e: Extinction rate per million year along branches; j: Likelihood of founder-event speciation at cladogenesis.

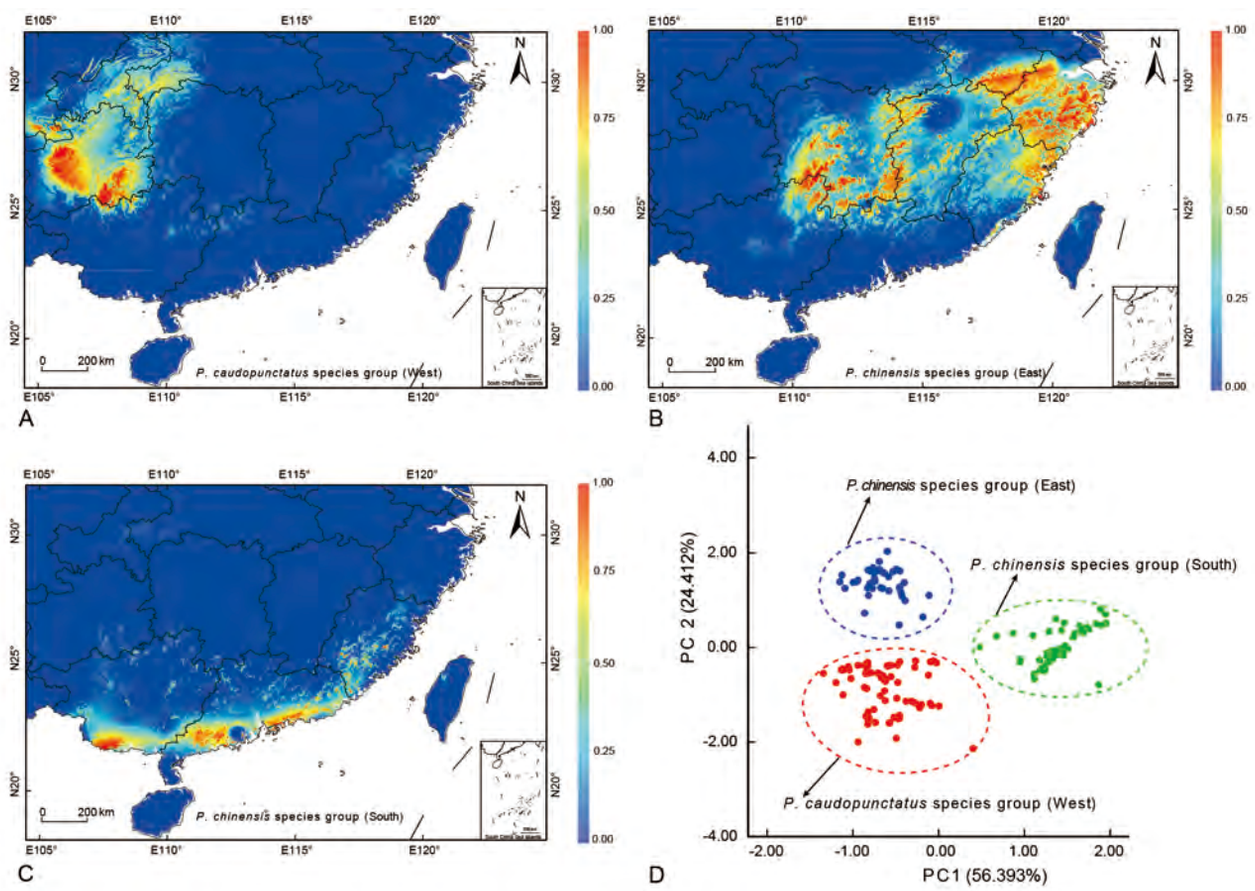

Figure 4 Ecological niche models based on six bioclimatic variables using Maxent predictions, suggesting suitable habitats for *P. caudopunctatus* and *P. chinensis* species groups were concentrated in West and South-East China, respectively, and a PCA scatter plot of 19 bioclimatic variables (PC1 vs. PC2)

A: Suitable habitat for *P. caudopunctatus* species group (West) in Guizhou and, to some extent, the Wuling Mountains (southeastern Chongqing, northwestern Hunan, and western Hubei). B: Suitable habitat for *P. chinensis* species group (East) in the Xuefeng Mountains, Nanling Mountains, Luoxiao Mountains, Wuyi-Tianmu Mountains, and Dabie Mountains. C: Suitable habitat for *P. chinensis* species group (South) in Shiwandashan Mountains, Yunwu Mountains, and Lianhua Mountains.

(West), *P. chinensis* (East), and *P. chinensis* species groups (South). Independent sample *t*-tests suggested that of the 19 bioclimatic variables, 10 were significantly different between West and East, 12 were significantly different between West and South, and eight were significantly different between East and South (P<0.05, Table 4).

DISCUSSION

Phylogeny and classification

Here, mitogenomes and 32 nuclear loci were concatenated into a data matrix for phylogenetic analysis of the genus *Paramesotriton*. The amount of molecular data and number of

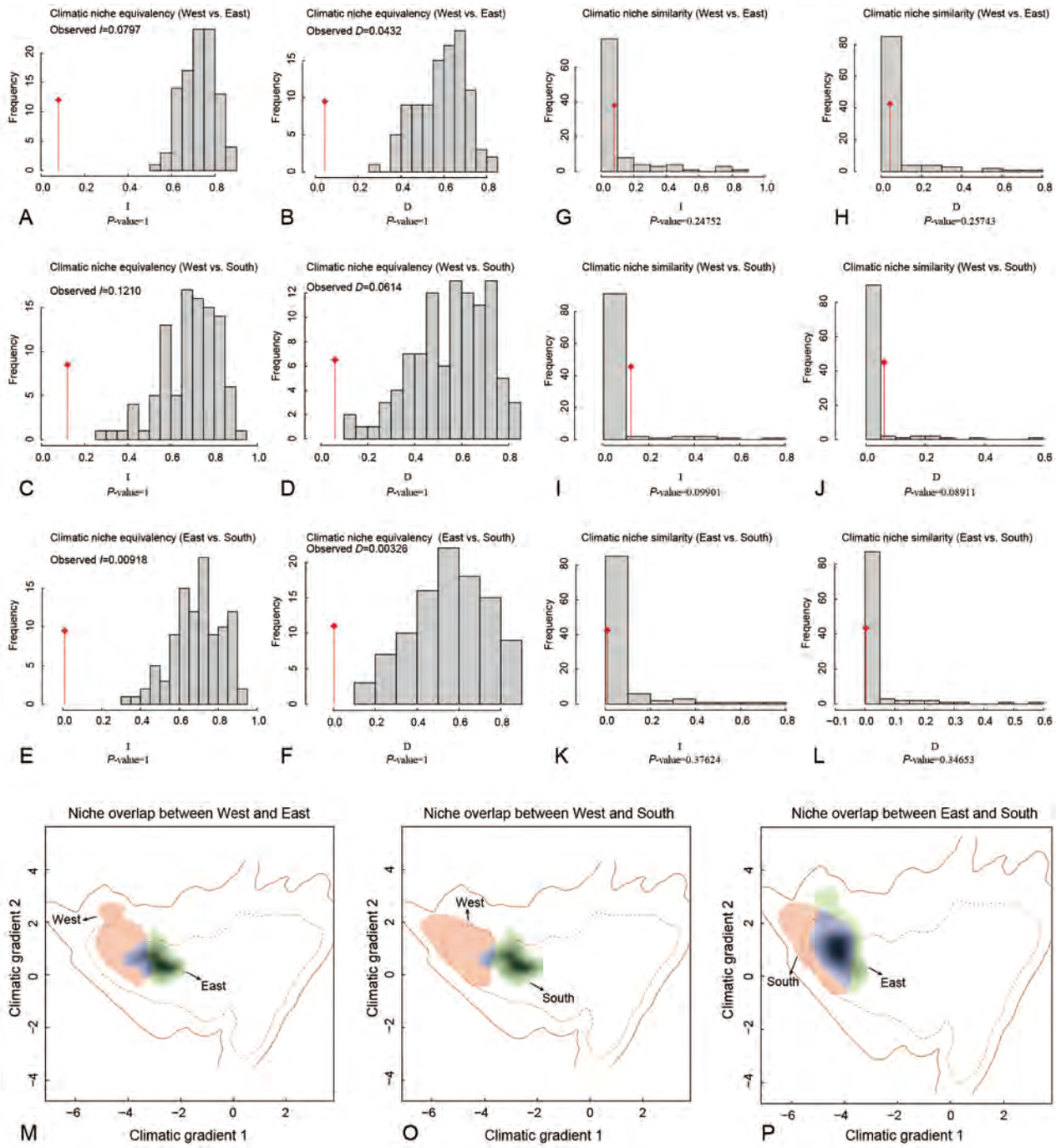

Figure 5 Climatic niche differentiation of *P. caudopunctatus* species group (West) and *P. chinensis* species group (East/South) in *Paramesotriton* in southern China

A–F: Histograms of niche equivalency distributions, where diamond lines represent observed values. G–L: Histograms of bidirectional niche similarity distributions. M–P: Species density for pairwise species comparisons along two climatic gradients. Solid red line denotes full range (100%) of climatic niche breadths for pairs of comparison species. Dashed red line denotes 50% of environmental density used to delineate the edge climate. Pink and green areas denote niche breadths for pairs of comparison species groups, blue denotes overlapping niche breadths.

samples analyzed exceeded all previous phylogenetic studies of the genus (Chan et al., 2001; Dubois et al., 2021; Gu et al., 2012a; Lu et al., 2004; Yuan et al., 2014; Zhang et al., 2008). Our analysis resolved a long-standing phylogenetic controversy concerning species groups and interspecific relationships (Figure 2). Overall, phylogenetic analysis highly supported the *P. chinensis* species group (subgenus *Paramesotriton*) and *P. caudopunctatus* species group (subgenera *Allomesotriton* and *Karstotriton*) previously proposed as monophyletic based on morphological characters

Table 3 Nineteen bioclimatic variables were used for principal component analysis (PCA) based on occurrence locations and eigenvalues greater than one

Bioclimatic variables	Component			
	1	2	3	4
BIO1 = Annual Mean Temperature	0.942	0.128	0.300	0.034
BIO2 = Mean Monthly Temperature Range	−0.254	−0.256	0.177	0.910
BIO3 = Isothermality	0.831	−0.381	−0.111	0.358
BIO4 = Temperature Seasonality	−0.900	0.340	0.183	−0.045
BIO5 = Max Temperature of Warmest Month	0.452	0.470	0.734	0.030
BIO6 = Min Temperature of Coldest Month	0.977	−0.033	0.179	−0.047
BIO7 = Temperature Annual Range	−0.905	0.310	0.209	0.073
BIO8 = Mean Temperature of Wettest Quarter	0.829	0.092	0.425	−0.154
BIO9 = Mean Temperature of Driest Quarter	0.944	0.218	0.175	0.044
BIO10 = Mean Temperature of Warmest Quarter	0.690	0.433	0.569	−0.009
BIO11 = Mean Temperature of Coldest Quarter	0.980	0.011	0.164	0.026
BIO12 = Annual Precipitation	0.661	0.589	−0.410	−0.004
BIO13 = Precipitation of Wettest Month	0.794	0.348	−0.448	0.087
BIO14 = Precipitation of Driest Month	−0.275	0.924	−0.135	0.047
BIO15 = Precipitation Seasonality	0.742	−0.599	−0.169	0.033
BIO16 = Precipitation of Wettest Quarter	0.855	0.230	−0.421	0.038
BIO17 = Precipitation of Driest Quarter	−0.205	0.944	−0.149	0.127
BIO18 = Precipitation of Warmest Quarter	0.888	0.118	−0.385	−0.036
BIO19 = Precipitation of Coldest Quarter	−0.135	0.951	−0.128	0.185
Eigenvalues	7.911	4.837	0.759	1.697
Percentage of total variance	56.393	24.412	11.176	5.573
Cumulative percentage	56.393	79.805	90.981	96.554

Principal components of these variables were used to compare climatic conditions at record sites of *P. caudopunctatus* and *P. chinensis* species groups.

Table 4 Independent sample *t*-tests based on 19 bioclimatic variables for occurrence locations of *P. caudopunctatus* and *P. chinensis* species groups

Bioclimatic variables	West vs. East		West vs. South		East vs. South	
	F	*P*-value	*F*	*P*-value	*F*	*P*-value
BIO1 = Annual Mean Temperature	0.258	0.612	1.621	0.205	0.484	0.488
BIO2 = Mean Monthly Temperature Range	5.721	0.018*	2.487	0.117	0.423	0.517
BIO3 = Isothermality	2.748	0.100	2.968	0.087	0.011	0.917
BIO4 = Temperature Seasonality	1.738	0.190	22.005	0.000*	30.357	0.000*
BIO5 = Max Temperature of Warmest Month	2.717	0.102	0.504	0.479	6.011	0.016*
BIO6 = Min Temperature of Coldest Month	0.090	0.765	2.287	0.133	1.138	0.289
BIO7 = Temperature Annual Range	8.938	0.003*	7.207	0.008*	29.653	0.000*
BIO8 = Mean Temperature of Wettest Quarter	27.846	0.000*	0.024	0.877	26.421	0.000*
BIO9 = Mean Temperature of Driest Quarter	0.307	0.581	4.834	0.030*	5.456	0.022*
BIO10 = Mean Temperature of Warmest Quarter	1.283	0.260	0.311	0.578	3.058	0.084
BIO11 = Mean Temperature of Coldest Quarter	0.582	0.447	4.513	0.036*	1.445	0.232
BIO12 = Annual Precipitation	6.114	0.015*	14.227	0.000*	1.428	0.235
BIO13 = Precipitation of Wettest Month	13.467	0.000*	30.463	0.000*	3.920	0.051
BIO14 = Precipitation of Driest Month	14.338	0.000*	32.566	0.000*	0.880	0.351
BIO15 = Precipitation Seasonality	21.897	0.000*	10.337	0.002*	2.225	0.139
BIO16 = Precipitation of Wettest Quarter	4.349	0.039*	31.657	0.000*	8.984	0.003*
BIO17 = Precipitation of Driest Quarter	13.648	0.000*	66.024	0.000*	5.861	0.017*
BIO18 = Precipitation of Warmest Quarter	3.320	0.071	35.426	0.000*	14.199	0.000*
BIO19 = Precipitation of Coldest Quarter	7.465	0.007*	14.445	0.000*	0.580	0.448

"*" denotes significant differences (P<0.05) between habitats of *P. caudopunctatus* and *P. chinensis* species groups in southern China.

(Fei et al., 2006; Fei & Ye, 2016).

Within the *P. caudopunctatus* species group, the phylogenetic relationships of species were well resolved, and the obtained topology was similar to previous studies (Gu et al., 2012a, 2012b; Luo et al., 2021; Yuan et al., 2014, 2016a). Due to the position of *P. labiatus*, the obtained *P. chinensis* species group phylogeny was inconsistent with previous tree topologies (Yuan et al., 2014, 2016a). Inferred from mitochondrial partial $tRNA^{Met}$, *ND2*, and flanking tRNAs ($tRNA^{Trp}$ and partial $tRNA^{Ala}$), the most likely position of *P. labiatus* was as sister taxon to all remaining members (*P. chinensis* and *P. hongkongensis*) of the *P. chinensis* species group except for *P. guangxiensis*, *P. deloustali*, and *P. fuzhongensis* (Wu et al., 2009; Supplementary Figure S1F), although this result was only weakly supported by partitioned ML, maximum parsimony, and BI. Using mitochondrial *ND2* and flanking tRNAs ($tRNA^{Trp}$ and partial $tRNA^{Ala}$), Yuan et al. (2014) identified *P. labiatus* as the sister taxon to all members of the *P. chinensis* species group with very high support. Using a similar molecular marker and partitioning strategy, Wu et al. (2010) and Yuan et al. (2016a) found that the phylogeny of the *P. chinensis* species group contained three polytomic clades, with *P. labiatus* at the bottom (Supplementary Figure S1I). Notably, although these studies shared the same molecular markers and similar analytical methods, except for number of sequences, the evolutionary models were different. In this study, the phylogenetic relationships within the *P. chinensis* species group were subclade B1 ((*P. deloustali*+(*P. guangxiensis*+(*P. yunwuensis*+*P. fuzhongensis*)))+(subclade B2 (*P. labiatus*)+subclade B3 ((*P. qixilingensis*+*P. chinensis*)+(*P. aurantius*+*P. hongkongensis*))), while *P. labiatus* was identified as a sister taxon to the remaining species of the *P. chinensis* species group identified in Yuan et al. (2014) or was unresolved (Yuan et al., 2016a). The reason for this was due to differences in the type and number of molecular markers (e.g., Yuan et al., 2014, 2016a only used mitochondrial *ND2* and its flanking tRNAs), as reflected in other amphibian studies (Wu et al., 2020; Yan et al., 2021). In conclusion, compared to previous studies (Wu et al., 2009, 2010; Yuan et al., 2014, 2016a), our phylogenetic tree provides good resolution of the interspecific phylogenetic positions of species within the genus *Paramesotriton*.

Hidden species diversity

Cryptic species may still be present in *Paramesotriton*. For example, Li et al. (2008a, 2008b) and Gu et al., (2012b) described *P. longliensis*, *P. zhijinensis*, and *P. maolanensis* from eastern Guizhou based on small mitochondrial differences. Wang et al. (2013) distinguished *P. wulingensis*, which was once regarded as *P. caudopunctatus*, and Yuan et al. (2016a) identified *P. aurantius* as a cryptic species found in geographic populations of *P. chinensis*. In general, one of the main criteria for phylogenetic species delineation is reciprocal monophyly (Kizirian & Donnelly, 2004). However, for species that have diverged recently or between which some gene flow exists, not all molecular markers will be monophyletic in the phylogenetic tree (Fujita et al., 2012; Hudson & Coyne, 2002).

Our analysis supported the presence of five hypothetical phylogenetic cryptic species in *P. longliensis* collected from Guizhou and Hubei, *P. deloustali* collected from Yunnan, and *P. hongkongensis* collected from Guangdong. Special submerged karst landscapes have revealed many cryptic species (Lefébure et al., 2006). Here, species of the *P. caudopunctatus* group were found mainly in karst caves and associated waterholes in western China. Within the *P. caudopunctatus* species group, genetic distances varied between the four *P. longliensis* populations, ranging from 0.52% to 1.83%. Overall, the genetic distances were close to the intrageneric genetic distances of *Paramesotriton*, e.g., 0.52%–0.92% between recognized *P. longliensis* and *P. maolanensis* and 0.59%–0.95% between three populations of *P. longliensis* and the type locality sequence. This suggests that the three populations of *P. longliensis* may represent three cryptic species with little genetic divergence but significant morphological differences (Li et al., 2008a, 2008b; Luo et al., 2021). Within the *P. chinensis* species group, the interspecific genetic distances for *P. deloustali* and *P. hongkongensis* were 1.05% and 2.19%, respectively, which are close to or greater than the interspecific genetic distances for other amphibians (e.g., 1.1% for *Hynobius formosanus* vs. *H. arisanensis* based on the mitogenome; Pan et al. 2019). Geographic isolation may be a major factor in the formation of these cryptic species, such as separation between the Guangdong (Chaoshan) and Hong Kong populations of *P. hongkongensis* by the Pearl River. Taken together, these results indicate that the biodiversity of the genus *Paramesotriton* remains underestimated. Future research will need to use genomics or population genetics with more loci and examine the rapid formation of new species through environmental adaptation (e.g., to karst habitats) or recent gene flow (Xu & Che, 2019).

Historical biogeography

In East Asia, breakthroughs in amphibian and reptile biogeography in the last decade suggest that geological and climatic changes since the Cenozoic have influenced biodiversity patterns in southern China (Che et al., 2010; Chen et al., 2018a, 2020; Guo et al., 2019, 2020; Hofmann et al., 2019; Li et al., 2013; Liang et al., 2018; Oliver et al., 2015; Yuan et al., 2016b, 2018; Wu et al., 2020; Zhou et al., 2021). However, comparatively little attention has been paid to tailed amphibians, especially salamanders. Geological changes in East Asia may have influenced the early evolutionary history of *Paramesotriton*. Dating analyses indicated that *Paramesotriton* originated about 25.42 Ma (95% HPD: 21.27–29.79 Ma) near the late Oligocene (Cohen et al., 2013), followed by early diversification and vicariance into two species groups during the early Miocene (ca. 22.86 Ma). This period coincides with geological events at the Oligocene/Miocene boundary, i.e., rapid lateral extrusion of Indochina (Tapponnier et al., 1990; Wang et al., 2006; Zhao et al., 2016), uplift of the Himalayan/QTP (An et al., 2006; Bai et al., 2010; Ding et al., 2017; Mulch & Chamberlain, 2006; Sun, 1997), and formation of karst landscapes in southwestern China (Che & Yu, 1985). The timing of this origin and estimated date of interspecific divergence are consistent with co-distributed species in East Asia, such as amphibians (Che et al., 2010; Chen et al., 2013; Wu et al., 2020; Zeng et al.,

2020), reptiles (Guo et al., 2020), plants (Deng et al., 2018; Sun et al., 2022; Xiang et al., 2016, 2021; Zhao et al., 2016), and invertebrates (Zhang & Li, 2013; Zhao & Li, 2017).

Subsequent lineage diversification of *Paramesotriton* during the mid-Miocene closely correlated with geological movement and climate change during that period. Diversification of the main lineages of the two *Paramesotriton* species groups first peaked in the mid-Miocene (nodes 2–6; Figure 3C), a period characterized by further rapid uplift of the Himalayan/QTP (ca. 20–10 Ma; Ding et al., 2017; Favre et al., 2015) and global climate decline (Miao et al., 2012; Westerhold et al., 2020; Zachos et al., 2001). The uninterrupted uplift of the eastern edge of the QTP (e.g., Hengduan Mountains) and the Wuyi-Nanling Mountains from the mid-Miocene (ca. 15–10 Ma) significantly altered the mountain landscape and river erosion patterns in the region (Favre et al., 2015; López-Pujol et al., 2011; Yan et al., 2018). This orogeny drove the establishment of the mountain and modern river systems, e.g., the Pearl River, Minjiang River, and lower Yangtze River (Yan et al., 2018; Zheng et al., 2013; Zheng, 2015), possibly contributing to lineage diversification of *Paramesotriton*, especially the *P. chinensis* species group. Orogeny in small regions may also have caused species diversification. Within the *P. caudopunctatus* species group, the mid-Miocene (node 2, Figure 3B) was divided into subclades A1 and A2 (Figure 2). The main geological event during this period was the equalization of the action of the Philippine Sea and Indian plates on the South China/Southeast Asian plate, which led to the slow uplift of the crust to form a low mountainous landscape with high western and low eastern edges, accompanied by regional-scale orogenic movements, including the formation of the ancient Wuling Mountains (Zhou & Chen, 1993). Geographical isolation due to the Wuling Mountains may have led to divergence of the *P. caudopunctatus* species group into two subclades, while the subsequent formation and westward development of the Miaoling in the early Pleistocene (Lin, 1993; Zhou & Chen, 1993) together with the warm and humid climate (Bureau of Geology and Mineral Guizhou Province, 1987; Ji, 1992; Li, 2001; Tong et al., 1994) likely promoted species diversification of the group. Thus, the combined effects of geology and climate change in East Asia from the mid-Miocene likely promoted diversification of species within *Paramesotriton*. Similar patterns of diversification have been found in other Asian amphibians, such as the Asian leaf-litter frog genus *Leptobrachella* (Chen et al., 2018a), Asian torrent frog genus *Amolops* (Wu et al., 2020; Zeng et al., 2020), and Asian knobby newt genus *Tylototriton* (Wang et al., 2018a). This common pattern suggests that amphibians distributed in southern China may have exhibited common evolutionary responses to the geological and climatic changes that occurred during the Miocene. Finally, the formation of *Paramesotriton* and the Yangtze River coincided closely, with species diversifying subsequent to the formation of the river (Favre et al., 2015; Fu et al., 2020; Zheng et al., 2013; Zheng, 2015). Thus, the low dispersal ability of the genus, geographic isolation of the Yangtze River, and limited movement ability of the species may be the main factors limiting the spread of *Paramesotriton* species north of the Yangtze River.

The rich species diversity (Hu et al., 2021; Myers et al., 2000), high endemism (Lei et al., 2015; Ma et al., 2019; Wang et al., 2017), and natural environment of southwestern China make it an important area for biologists studying the origins of species diversity in East Asia. Ancestral area reconstruction and spatiotemporal analysis suggested that the ancestors of the genus *Paramesotriton* may have originated in the karst areas of southwestern China (Yunnan-Guizhou Plateau/South China), as reported previously for cave fish (Wen et al., 2022; Zhao & Zhang, 2009), frogs (Ye & Fei, 2001; Yuan et al., 2016b; Zhou et al., 2017), and snakes (Guo et al., 2020). According to the current geographic distribution and phylogenetic tree, we propose a "vicariance-dispersal-vicariance" hypothesis for the evolutionary history of *Paramesotriton*. The highly heterogeneous habitats created by the intense uplift of the QTP, rapid lateral extrusion of Indochina, and karst landscape formation led to the isolation and splitting of ancestral species of *Paramesotriton* into the West and South/East clades. The West Clade, corresponding to the *P. caudopunctatus* species group, contributed to species formation in and around Guizhou after dispersal and vicariance. The ancestors of the East Clade, corresponding to the *P. chinensis* species group, dispersed from southern to eastern China and contributed to species formation after vicariance. The subsequent East-to-South dispersal event also explains the narrow sympatric distribution of several species in the east. In addition, considering the special geographic location and long natural evolutionary history of southwestern China, the West-South-East geographic distribution and phylogenetic patterns suggest a West-to-East dispersal pattern for *Paramesotriton* (Figures 1, 3). As this dispersal pattern has also been found in some snakes (Guo et al., 2011, 2016, 2020) and frogs (Yan et al., 2021; Yuan et al., 2016; Zhou et al., 2017) in southern China, a West-to-East dispersal pattern may be widely present in other taxa in southern China, although there are some exceptions showing East-to-West dispersal (Liang et al., 2018).

We note that recent evolutionary radiation may have occurred in the *P. caudopunctatus* species group, triggering rapid adaptation to the karst environment, and accelerating the formation of cryptic species. However, genomic studies are needed to reveal the complete evolutionary history and adaptive mechanisms.

Environmental heterogeneity and spatial distribution

Environmental factors play important roles in driving speciation, spatial distribution, and adaptation (Antonelli et al., 2018; Pereira & Wake, 2009; Vieites et al., 2007). To understand the phylogenetic differences in geographic distribution from West-to-East and North-to-South, we tested the influence of environmental heterogeneity on the spatial distribution of salamander species in southern China. Based on bioclimatic variables, PCA, independent sample *t*-tests, and niche differentiation analysis revealed significantly different habitat environmental conditions and some climatic ecological niche differentiation among the three regions (Table 3; Figure 4). In terms of physical geography, the *Paramesotriton* distribution area belongs to the eastern monsoon region of China (Zhang, 2011), while the western

and eastern regions belong to the mid-subtropics (including the coasts of Zhejiang and Fujian reaching westward to the Yunnan-Guizhou Plateau) and the southern part belongs to the south subtropics (including southern Fujian, Guangxi, Guangdong, and Yunnan), which differ significantly in terms of climate, rainfall, and topography. Climatically, southwestern and southeastern China are influenced by the warm and wet monsoon from the Indian Ocean and the Asian monsoon from the Pacific Ocean (An et al., 2001; Jiang & Ding, 2009; Ren et al., 2021; Vornlocher et al., 2021; Wan et al., 2007). Zoogeographically, in southern China, there are different divisions between the eastern (Eastern Hillock Plain sub-region) and western (Western Mountainous Plateau sub-region) parts of Central China of the Oriental Realm, and the southern part of South China (Min'guang Coastal sub-region) (Xing et al., 2008; Zhang, 2011). Geomorphologically, the West region is a fully developed, high-coverage karst landscape, whereas the East region is almost karst-free, and the South region is a poorly covered karst landscape (Goldscheider et al., 2020; Zhang, 1980). Ecological differentiation and environmental adaptation are considered to play important roles in driving species differentiation and formation (McCulloch et al., 2021; Nosil, 2012; Rundle & Nosil, 2005; Wang et al., 2018b). Here, the species distribution model predictions suggested that the *P. caudopunctatus* and *P. chinensis* species groups only have suitable habitat in West, East, and South China (Figure 4). The combination of these factors may reflect adaptive responses of salamanders to the microhabitat of the location of occurrence in the current climatic scenario. Although we still know little about the adaptive mechanisms of *Paramesotriton* in different ecoregions in southern China at the morphological and genetic levels, it appears that the western and eastern landscapes and resulting ecological changes are closely correlated with the evolution of West-to-East divergence (Guo et al., 2020; Yan et al., 2021). Future research should focus on the adaptation of *Paramesotriton* to karst water environments, conservation biology, and population genetic diversity, which are important for understanding the adaptation of amphibians to water environments and global climate change.

CONCLUSIONS

We investigated the phylogeny, biogeography, environmental variation, and geographic distribution patterns of the mountain salamander genus *Paramesotriton* based on a sample set covering 14 species, combined with mitogenomic and nuclear gene data. The phylogeny and monophyly of the genus and its two species groups, *P. caudopunctatus* and *P. chinensis* species groups, were determined, and five phylogenetic cryptic species were identified. Biogeographic analyses suggested that *Paramesotriton* originated in southwestern China (Yunnan-Guizhou Plateau/South China) in the late Oligocene, with subsequent dispersal from South China northward to East China, forming West-South-East geographic distribution patterns in terrains II and III in South China. Based on bioclimatic variation and interspecific geographic distribution patterns, we suggest that the natural landscape of karst mountains in southern China and changes in ecological factors played important roles in the evolution of *Paramesotriton* from West-to-East and the formation of the West-South-East distribution pattern.

SCIENTIFIC FIELD SURVEY PERMISSION INFORMATION

All samples were obtained following Chinese regulations for the Implementation of the Protection of Terrestrial Wild Animals (State Council Decree (1992) No. 13), and the Guidelines for the Care and Use of Laboratory Animals by the Ethics Committee at Guizhou Normal University (Guiyang, Guizhou, China).

SUPPLEMENTARY DATA

Supplementary data to this article can be found online.

COMPETING INTERESTS

The authors declare that they have no competing interests.

AUTHORS' CONTRIBUTIONS

J.Z. and T.L. conceived and designed the research; T.L., Y.S.S., N.X., J.J.Z., X.L.W., W.C.C., and B.W.Z. conducted field surveys and collected samples; T.L., N.X., and B.W.Z. performed molecular work; T.L. H.Q.D., and S.S.Y. analyzed molecular and environmental data; T.L., Y.S.S., J.Z., and H.Q.D. wrote, discussed, and revised the manuscript. All authors read and approved the final version of the manuscript.

ACKNOWLEDGEMENTS

We are grateful to Prof. Zhi-Yong Yuan, Prof. Xiao-Ming Gu, and Dr. Xiao-Long Liu for providing tissue samples used for molecular analysis. We thank Kai Gao, Xiang Zeng, Jun Zhou, Hong-Tao Cui, Xiang-Di Fan, Ya-Li Wang, and Si-Wei Wang for their help during sample collection. We thank LetPub (www.letpub.com) for its linguistic assistance during manuscript preparation.

REFERENCES

Allouche O, Tsoar A, Kadmon R. 2006. Assessing the accuracy of species distribution models: prevalence, kappa and the true skill statistic (TSS). *Journal of Applied Ecology*, **43**(6): 1223−1232.

AmphibiaChina. 2022. The database of Chinese amphibians. Yunnan, China: Kunming Institute of Zoology. http://www.amphibiachina.org/. (in Chinese)

An ZS, Kutzbach JE, Prell WL, Porter SC. 2001. Evolution of Asian monsoons and phased uplift of the Himalaya–Tibetan plateau since Late Miocene times. *Nature*, **411**(6833): 62−66.

An ZS, Zhang PZ, Wang EQ, Wang SM, Qiang XK, Li L, et al. 2006. Changes of the monsoon-arid environment in China and growth of the Tibetan Plateau since the Miocene. *Quaternary Sciences*, **26**(5): 678−693. (in Chinese)

Allen GC, Flores-Vergara MA, Krasynanski S, Kumar S, Thompson WF. 2006. A modified protocol for rapid DNA isolation from plant tissues using cetyltrimethylammonium bromide. *Nature Protocols*, **1**(5): 2320−2325.

Antonelli A, Kissling WD, Flantua SGA, Bermúdez MA, Mulch A, Muellner-Riehl AN, et al. 2018. Geological and climatic influences on mountain

biodiversity. *Nature Geoscience*, **11**(10): 718−725.
Bai DH, Unsworth M, Meju MA, Ma XB, Teng JW, Kong XR, et al. 2010. Crustal deformation of the eastern Tibetan plateau revealed by magnetotelluric imaging. *Nature Geoscience*, **3**(5): 358−362.
Bankevich A, Nurk S, Antipov D, Gurevich AA, Dvorkin M, Kulikov AS, et al. 2012. SPAdes: a new genome assembly algorithm and its applications to single-cell sequencing. *Journal of Computational Biology*, **19**(5): 455−477.
Bernt M, Donath A, Jühling F, Externbrink F, Florentz C, Fritzsch G, et al. 2013. MITOS: improved *de novo* metazoan mitochondrial genome annotation. *Molecular Phylogenetics and Evolution*, **69**(2): 313−319.
Bouckaert R, Heled J, Kühnert D, Vaughan T, Wu CH, Xie D, et al. 2014. BEAST 2: a software platform for bayesian evolutionary analysis. *PLoS Computational Biology*, **10**(4): e1003537.
Broennimann O, Fitzpatrick MC, Pearman PB, Petitpierre B, Pellissier L, Yoccoz NG, et al. 2012. Measuring ecological niche overlap from occurrence and spatial environmental data. *Global Ecology and Biogeography*, **21**(4): 481−497.
Bureau of Geology and Mineral Guizhou Province. 1987. Regional Geology of Guizhou Province. Beijing: Geological Publishing House. (in Chinese)
Chan LM, Zamudio KR, Wake DB. 2001. Relationships of the salamandrid genera *Paramesotriton, Pachytriton*, and *Cynops* based on mitochondrial DNA sequences. *Copeia*, **2001**(4): 997−1009.
Chang MLY. 1935. Note préliminaire sur la classification des salamandres d'asie orientale. *Bulletin de la Société Zoologique de France*, **60**: 424−427.
Che J, Zhou WW, Hu JS, Yan F, Papenfuss TJ, Wake DB, et al. 2010. Spiny frogs (Paini) illuminate the history of the Himalayan region and Southeast Asia. *Proceedings of the National Academy of Sciences of the United States of America*, **107**(31): 13765−13770.
Che YT, Yu JZ. 1985. Karst in China. Beijing: Science Press. (in Chinese)
Chen JM, Poyarkov Jr NA, Suwannapoom C, Lathrop A, Wu YH, Zhou WW, et al. 2018a. Large-scale phylogenetic analyses provide insights into unrecognized diversity and historical biogeography of Asian leaf-litter frogs, genus *Leptolalax* (Anura: Megophryidae). *Molecular Phylogenetics and Evolution*, **124**: 162−171.
Chen JM, Prendini E, Wu YH, Zhang BL, Suwannapoom C, Chen HM, et al. 2020. An integrative phylogenomic approach illuminates the evolutionary history of Old World tree frogs (Anura: Rhacophoridae). *Molecular Phylogenetics and Evolution*, **145**: 106724.
Chen XH, Chen Z, Jiang JP, Qiao L, Lu YQ, Zhou KY, et al. 2013. Molecular phylogeny and diversification of the genus *Odorrana* (Amphibia, Anura, Ranidae) inferred from two mitochondrial genes. *Molecular Phylogenetics and Evolution*, **69**(3): 1196−1202.
Chen YX, Chen YS, Shi CM, Huang ZB, Zhang Y, Li SK, et al. 2018b. SOAPnuke: a MapReduce acceleration-supported software for integrated quality control and preprocessing of high-throughput sequencing data. *GigaScience*, **7**(1): gix120.
Cobos ME, Peterson AT, Barve N, Osorio-Olvera L. 2019. Kuenm: an R package for detailed development of ecological niche models using Maxent. *PeerJ*, **7**: e6281.
Cohen KM, Finney SC, Gibbard PL, Fan JX. 2013. The ICS international chronostratigraphic chart. *Episodes*, **36**(3): 199−204.
Deng M, Jiang XL, Hipp AL, Manos PS, Hahn M. 2018. Phylogeny and biogeography of East Asian evergreen oaks (*Quercus* section *Cyclobalanopsis*; Fagaceae): insights into the Cenozoic history of evergreen broad-leaved forests in subtropical Asia. *Molecular Phylogenetics and Evolution*, **119**: 170−181.
Di Cola V, Broennimann O, Petitpierre B, Breiner FT, D'Amen M, Randin C, et al. 2017. ecospat: an R package to support spatial analyses and modeling of species niches and distributions. *Ecography*, **40**(6): 774−787.
Ding L, Spicer RA, Yang J, Xu Q, Cai FL, Li S, et al. 2017. Quantifying the rise of the Himalaya orogen and implications for the South Asian monsoon. *Geology*, **45**(3): 215−218.
Dormann CF, Elith J, Bacher S, Buchmann C, Carl G, Carré G, et al. 2013. Collinearity: a review of methods to deal with it and a simulation study evaluating their performance. *Ecography*, **36**(1): 27−46.
Dubois A, Ohler A, Pyron RA. 2021. New concepts and methods for phylogenetic taxonomy and nomenclature in zoology, exemplified by a new ranked cladonomy of recent amphibians (Lissamphibia). *Megataxa*, **5**(1): 1−738.
Dubois A, Raffaëlli J. 2009. A new ergotaxonomy of the family Salamandridae Goldfuss, 1820 (Amphibia, Urodela). *Alytes*, **26**(1–4): 1–85.
Estes R. 1981. Gymnophiona, Caudata: Handbuch der Paläoherpetologie. New York: Gustav Fischer.
Favre A, Päckert M, Pauls SU, Jähnig SC, Uhl D, Michalak I, et al. 2015. The role of the uplift of the Qinghai-Tibetan Plateau for the evolution of Tibetan biotas. *Biological Reviews*, **90**(1): 236−253.
Fei L, Hu SQ, Ye CY, Huang YZ. 2006. Fauna Sinica, Amphibia, vol. 1. Beijing: Science Press. (in Chinese)
Fei L, Ye CY. 2016. Amphibians of China, Volume 1. Beijing: Science Press.
Frost DR. 2021. Amphibian Species of the World: an Online Reference. Version 6.0. New York: American Museum of Natural History. http://research.amnh.org/herpetology/amphibia/index.html.
Fu XW, Zhu WL, Geng JH, Yang SY, Zhong K, Huang XT, et al. 2020. The present-day Yangtze River was established in the late miocene: evidence from detrital zircon ages. *Journal of Asian Earth Sciences*, **205**: 104600.
Fujita MK, Leaché AD, Burbrink FT, McGuire JA, Moritz C. 2012. Coalescent-based species delimitation in an integrative taxonomy. *Trends in Ecology & Evolution*, **27**(9): 480−488.
Goldscheider N, Chen Z, Auler AS, Bakalowicz M, Broda S, Drew D, et al. 2020. Global distribution of carbonate rocks and karst water resources. *Hydrogeology Journal*, **28**(5): 1661−1677.
Gu XM, Chen RR, Tian YZ, Li S, Ran JC. 2012b. A new species of *Paramesotriton* (Caudata: Salamandridae) from Guizhou Province, China. *Zootaxa*, **3510**(1): 41−52.
Gu XM, Wang H, Chen RR, Tian YZ, Li S. 2012a. The phylogenetic relationships of *Paramesotriton* (Caudata: Salamandridae) based on partial mitochondrial DNA gene sequences. *Zootaxa*, **3150**(1): 59−68.
Guisan A, Thuiller W. 2005. Predicting species distribution: offering more than simple habitat models. *Ecology Letters*, **8**(9): 993−1009.
Guo P, Liu Q, Li C, Chen X. Jiang K, Wang YZ, et al. 2011. Molecular phylogeography of Jerdon's pitviper (*Protobothrops jerdonii*): importance of the uplift of the Tibetan plateau. *Journal of Biogeography*, **38**(12): 2326−2336.
Guo P, Liu Q, Zhu F, Zhong GH, Che J, Wang P, et al. 2019. Multilocus phylogeography of the brown-spotted pitviper *Protobothrops mucrosquamatus* (Reptilia: Serpentes: Viperidae) sheds a new light on the diversification pattern in Asia. *Molecular Phylogenetics and Evolution*, **133**: 82−91.
Guo P, Liu Q, Zhu F, Zhong GH, Chen X, Myers EA, et al. 2016. Complex longitudinal diversification across South China and Vietnam in Stejneger's pit viper, *Viridovipera stejnegeri* (Schmidt, 1925) (Reptilia: Serpentes: Viperidae). *Molecular Ecology*, **25**(12): 2920−2936.
Guo P, Zhu F, Liu Q, Wang P, Che J, Nguyen TQ. 2020. Out of the hengduan mountains: molecular phylogeny and historical biogeography of the Asian water snake genus *Trimerodytes* (Squamata: Colubridae).

Molecular Phylogenetics and Evolution, **152**: 106927.
Hanley JA, McNeil BJ. 1982. The meaning and use of the area under a receiver operating characteristic (ROC) curve. *Radiology*, **143**(1): 29−36.
Hazzi NA, Moreno JS, Ortiz-Movliav C, Palacio RD. 2018. Biogeographic regions and events of isolation and diversification of the endemic biota of the tropical Andes. *Proceedings of the National Academy of Sciences of the United States of America*, **115**(31): 7985−7990.
Hijmans RJ, Cameron SE, Parra JL, Jones PG, Jarvis A. 2005a. Very high resolution interpolated climate surfaces for global land areas. *International Journal of Climatology*, **25**(15): 1965−1978.
Hijmans RJ, Guarino L, Jarvis A, O'Brien R, Mathur P, Bussink C, et al. 2005b. DIVA-GIS, version 5.2.https://manualzilla.com/doc/5743142/diva-gis-manual.
Hoang DT, Chernomor O, Von Haeseler A, Minh BQ, Vinh LS. 2018. UFBoot2: improving the ultrafast bootstrap approximation. *Molecular Biology and Evolution*, **35**(2): 518−522.
Hofmann S, Baniya CB, Litvinchuk SN, Miehe G, Li JT, Schmidt J. 2019. Phylogeny of spiny frogs *Nanorana* (Anura: Dicroglossidae) supports a Tibetan origin of a Himalayan species group. *Ecology and Evolution*, **9**(24): 14498−14511.
Hu YB, Fan HZ, Chen YH, Chang J, Zhan XJ, Wu H, et al. 2021. Spatial patterns and conservation of genetic and phylogenetic diversity of wildlife in China. *Science Advances*, **7**(4): eabd5725.
Hudson RR, Coyne JA. 2002. Mathematical consequences of the genealogical species concept. *Evolution*, **56**(8): 1557−1565.
IUCN. 2022[2021-01-20]. The IUCN Red List of Threatened Species. Version 2020-3. http://www.iucnredlist.org.
Ji RA. 1992. Evolution of quaternary natural environment in Guizhou. *Geology of Guizhou*, **9**(1): 59−62. (in Chinese)
Jiang H, Ding Z. 2009. Spatial and temporal characteristics of Neogene palynoflora in China and its implication for the spread of steppe vegetation. *Journal of Arid Environments*, **73**(9): 765−772.
Katoh K, Standley DM. 2013. MAFFT multiple sequence alignment software version 7: improvements in performance and usability. *Molecular Biology and Evolution*, **30**(4): 772−780.
Kieren S, Sparreboom M, Hochkirch A, Veith M. 2018. A biogeographic and ecological perspective to the evolution of reproductive behaviour in the family Salamandridae. *Molecular Phylogenetics and Evolution*, **121**: 98−109.
Kizirian D, Donnelly MA. 2004. The criterion of reciprocal monophyly and classification of nested diversity at the species level. *Molecular Phylogenetics and Evolution*, **32**(3): 1072−1076.
Kumar S, Stecher G, Tamura K. 2016. MEGA7: molecular evolutionary genetics analysis version 7.0 for bigger datasets. *Molecular Biology and Evolution*, **33**(7): 1870−1874.
Lanfear R, Frandsen PB, Wright AM, Senfeld T, Calcott B. 2017. PartitionFinder 2: new methods for selecting partitioned models of evolution for molecular and morphological phylogenetic analyses. *Molecular Biology and Evolution*, **34**(3): 772−773.
Lefébure T, Douady CJ, Gouy M, Trontelj P, Briolay J, Gibert J. 2006. Phylogeography of a subterranean amphipod reveals cryptic diversity and dynamic evolution in extreme environments. *Molecular Ecology*, **15**(7): 1797−1806.
Lei F, Qu YH, Song G, Alström P, Fjeldså J. 2015. The potential drivers in forming avian biodiversity hotspots in the East Himalaya Mountains of Southwest China. *Integrative Zoology*, **10**(2): 171−181.
Li JT, Li Y, Klaus S, Rao DQ, Hillis DM, Zhang YP. 2013. Diversification of rhacophorid frogs provides evidence for accelerated faunal exchange between India and Eurasia during the Oligocene. *Proceedings of the National Academy of Sciences of the United States of America*, **110**(9): 3441−3446.
Li S, Tian YZ, Gu XM. 2008a. A new species of the genus *Paramesotriton* (Caudata, Salamandridae). *Acta Zootaxonomica Sinica*, **33**(2): 410−413. (in Chinese)
Li S, Tian YZ, Gu XM, Xiong RC. 2008b. A new species of *Paramesotriton*— *Paramesotriton longliensis* (Caudata: Salamandridae). *Zoological Research*, **29**(3): 313−317. (in Chinese)
Li XZ. 2001. Evolution of karst geomorphology of Upper-Cenozoic and its influential factors in Guizhou plateau. *Guizhou Geology*, **18**(1): 29−36. (in Chinese)
Liang B, Zhou RB, Liu YL, Chen B, Lee Grismer L, Wang N. 2018. Renewed classification within *Goniurosaurus* (Squamata: Eublepharidae) uncovers the dual roles of a continental island (Hainan) in species evolution. *Molecular Phylogenetics and Evolution*, **127**: 646−654.
Lin SJ. 1993. The main features of tectonic movement of Late Cenozoic era in Guizhou. *Geology of Guizhou*, **10**(1): 10−17. (in Chinese)
López-Pujol J, Zhang FM, Sun HQ, Ying TS, Ge S. 2011. Centres of plant endemism in China: places for survival or for speciation?. *Journal of Biogeography*, **38**(7): 1267−1280.
Low BW, Zeng YW, Tan HH, Yeo DCJ. 2021. Predictor complexity and feature selection affect Maxent model transferability: evidence from global freshwater invasive species. *Diversity and Distributions*, **27**(3): 497−511.
Lu SQ, Yuan ZG, Pang JF, Yang DT, Yu FH, McGuire P, et al. 2004. Molecular phylogeny of the genus *Paramesotriton* (Caudata: Salamandridae). *Biochemical Genetics*, **42**(5): 139−148.
Luo T, Wen HM, Gao K, Zhou J, Zhou J. 2021. Phylogeography and cryptic species diversity of *Paramesotriton caudopunctatus* species group (Salamandridae: *Paramesotriton*) in Guizhou, China. *Asian Herpetological Research*, **12**(2): 188−200.
Ma L, Zhao YH, Yang JX. 2019. Cavefish of China. *In*: White WB, Culver DC, Pipan T. Encyclopedia of Caves. 3rd ed. London: Academic Press.
Matzke NJ. 2013. BioGeoBEARS: bioGeography with Bayesian (and likelihood) Evolutionary Analysis in R Scripts. Berkeley: University of California.
McCulloch GA, Foster BJ, Dutoit L, Harrop TWR, Guhlin J, Dearden PK, et al. 2021. Genomics reveals widespread ecological speciation in flightless insects. *Systematic Biology*, **70**(5): 863−876.
Miao YF, Herrmann M, Wu FL, Yan XL, Yang SL. 2012. What controlled mid–late Miocene long-term aridification in central Asia?—global cooling or Tibetan plateau uplift: a review. *Earth-Science Reviews*, **112**(3−4): 155−172.
Minh BQ, Anh M, Nguyen T, von Haeseler A. 2013. Ultrafast approximation for phylogenetic bootstrap. *Molecular Biology and Evolution*, **30**(5): 1188−1195.
Ministry of Environmental Protection. 2015. Priority areas for biodiversity conservation in China. Beijing: Ministry of Environmental Protection. (in Chinese)
Morales NS, Fernández IC, Baca-González V. 2017. MaxEnt's parameter configuration and small samples: are we paying attention to recommendations? A systematic review. *PeerJ*, **5**: e3093.
Mulch A, Chamberlain CP. 2006. The rise and growth of Tibet. *Nature*, **439**(7077): 670−671.
Myers N, Mittermeier RA, Mittermeier CG, Da Fonseca GAB, Kent J. 2000. Biodiversity hotspots for conservation priorities. *Nature*, **403**(6772): 853−858.

Nguyen LT, Schmidt HA, Von Haeseler A, Minh BQ. 2015. IQ-TREE: a fast and effective stochastic algorithm for estimating maximum-likelihood phylogenies. *Molecular Biology and Evolution*, **32**(1): 268−274.

Nosil P. 2012. Ecological Speciation. Oxford: Oxford University Press.

Oliver LA, Prendini E, Kraus F, Raxworthy CJ. 2015. Systematics and biogeography of the *Hylarana* frog (Anura: Ranidae) radiation across tropical Australasia, Southeast Asia, and Africa. *Molecular Phylogenetics and Evolution*, **90**: 176−192.

Pan T, Sun ZL, Lai XL, Orozcoterwengel P, Yan P, Wu GY, et al. 2019. Hidden species diversity in *Pachyhynobius*: a multiple approaches species delimitation with mitogenomes. *Molecular Phylogenetics and Evolution*, **137**: 138−145.

Pereira RJ, Wake DB. 2009. Genetic leakage after adaptive and nonadaptive divergence in the *Ensatina eschscholtzii* ring species. *Evolution*, **63**(9): 2288−2301.

Peterson AT, Nakazawa Y. 2008. Environmental data sets matter in ecological niche modelling: an example with *Solenopsis invicta* and *Solenopsis richteri*. *Global Ecology and Biogeography*, **17**(1): 135–144.

Phillips SJ, Anderson RP, Schapire RE. 2006. Maximum entropy modeling of species geographic distributions. *Ecological Modelling*, **190**(3–4): 231–259.

Phillips SJ, Dudík M. 2008. Modeling of species distributions with Maxent: new extensions and a comprehensive evaluation. *Ecography*, **31**(2): 161−175.

Radosavljevic A, Anderson RP. 2014. Making better MAXENT models of species distributions: complexity, overfitting and evaluation. *Journal of Biogeography*, **41**(4): 629−643.

Rahbek C, Borregaard MK, Antonelli A, Colwell RK, Holt BG, Nogues-Bravo D, et al. 2019b. Building mountain biodiversity: geological and evolutionary processes. *Science*, **365**(6458): 1114−1119.

Rahbek C, Borregaard MK, Colwell RK, Dalsgaard B, Holt BG, Morueta-Holme N, et al. 2019a. Humboldt's enigma: what causes global patterns of mountain biodiversity?. *Science*, **365**(6458): 1108−1113.

Rambaut A. 2016. FigTree v1.4. 3. http://tree.bio.ed.ac.uk/software/figtree/.

Rambaut A, Drummond AJ. 2010. TreeAnnotator version 1.8. http://beast.community/programs.

Rambaut A, Drummond AJ, Xie D, Baele G, Suchard MA. 2018. Posterior summarization in Bayesian phylogenetics using Tracer 1.7. *Systematic Biology*, **67**(5): 901−904.

Ren JB, Schubert BA, Lukens WE, Quan C. 2021. Low oxygen isotope values of fossil cellulose indicate an intense monsoon in East Asia during the late Oligocene. *Palaeogeography, Palaeoclimatology, Palaeoecology*, **577**: 110556.

Ronquist F, Teslenko M, van der Mark P, Ayres DL, Darling A, Höhna S, et al. 2012. MrBayes 3.2: efficient Bayesian phylogenetic inference and model choice across a large model space. *Systematic Biology*, **61**(3): 539−542.

Rundle HD, Nosil P. 2005. Ecological speciation. *Ecology Letters*, **8**(3): 336−352.

Schoener TW. 1968. The anolis lizards of Bimini: resource partitioning in a complex fauna. *Ecology*, **49**(4): 704−726.

Sun HL. 1997. Research of the Formation, Environment Change on Qinghai-Xizang (Tibetan) Plateau. Changsha: Hunan Science and Technology Press. (in Chinese)

Sun QH, Morales-Briones DF, Wang HX, Landis JB, Wen J, Wang HF. 2022. Phylogenomic analyses of the East Asian endemic *Abelia* (Caprifoliaceae) shed insights into the temporal and spatial diversification history with widespread hybridization. *Annals of Botany*, **129**(2): 201−216.

Swets JA. 1988. Measuring the accuracy of diagnostic systems. *Science*, **240**(4857): 1285−1293.

Tapponnier P, Lacassin R, Leloup PH, Schärer U, Dalai Z, Haiwei W, et al. 1990. The Ailao Shan/Red River metamorphic belt: tertiary left-lateral shear between Indochina and South China. *Nature*, **343**(6257): 431−437.

Tong GB, Zhang JP, Yang XD, Luo BX, Wang YZ, Chen PY. 1994. Late cenozoic palynoflora and environment changes in Yunnan-guizhou plateau. *Marine Geology & Quaternary Geology*, **14**(3): 92−104. (in Chinese)

Vieites DR, Min MS, Wake DB. 2007. Rapid diversification and dispersal during periods of global warming by plethodontid salamanders. *Proceedings of the National Academy of Sciences of the United States of America*, **104**(50): 19903−19907.

Vornlocher JR, Lukens WE, Schubert BA, Quan C. 2021. Late Oligocene precipitation seasonality in East Asia based on $\delta^{13}C$ profiles in fossil wood. *Paleoceanography and Paleoclimatology*, **36**(4): e2021PA004229.

Wan SM, Li AC, Clift PD, Stuut JBW. 2007. Development of the East Asian monsoon: mineralogical and sedimentologic records in the northern South China Sea since 20 Ma. *Palaeogeography, Palaeoclimatology, Palaeoecology*, **254**(3–4): 561–582.

Wang B, Huang Y, Li JT, Dai Q, Wang YZ, Yang DD. 2018b. Amphibian species richness patterns in karst regions in southwest China and its environmental associations. *Biodiversity Science*, **26**(9): 941−950. (in Chinese)

Wang B, Nishikawa K, Matsui M, Nguyen TQ, Xie F, Li C, et al. 2018a. Phylogenetic surveys on the newt genus *Tylototriton sensu lato* (Salamandridae, Caudata) reveal cryptic diversity and novel diversification promoted by historical climatic shifts. *PeerJ*, **6**: e4384.

Wang C, Tian YZ, Gu XM. 2013. A new species of the genus *Paramesotriton* (Caudata, Salamandridae). *Acta Zootaxonomica Sinica*, **38**(2): 388−397. (in Chinese)

Wang J, Ai B, Kong HH, Kang M. 2017. Speciation history of a species complex of *Primulina eburnea* (Gesneriaceae) from limestone karsts of southern China, a biodiversity hot spot. *Evolutionary Applications*, **10**(9): 919−934.

Wang YJ, Fan WM, Zhang YH, Peng TP, Chen XY, Xu YG. 2006. Kinematics and $^{40}Ar/^{39}Ar$ geochronology of the Gaoligong and Chongshan shear systems, western Yunnan, China: implications for early Oligocene tectonic extrusion of SE Asia. *Tectonophysics*, **418**(3–4): 235–254.

Warren DL, Glor RE, Turelli M. 2008. Environmental niche equivalency versus conservatism: quantitative approaches to niche evolution. *Evolution*, **62**(11): 2868−2883.

Warren DL, Glor RE, Turelli M. 2010. ENMTools: a toolbox for comparative studies of environmental niche models. *Ecography*, **33**(3): 607−611.

Wen HM, Luo T, Wang YL, Wang SW, Liu T, Xiao N, et al. 2022. Molecular phylogeny and historical biogeography of the cave fish genus *Sinocyclocheilus* (Cypriniformes: Cyprinidae) in southwest China. *Integrative Zoology*, **17**(2): 311−325.

Westerhold T, Marwan N, Drury AJ, Liebrand D, Agnini C, Anagnostou E, et al. 2020. An astronomically dated record of Earth's climate and its predictability over the last 66 million years. *Science*, **369**(6509): 1383−1387.

Wu YH, Yan F, Stuart BL, Prendini E, Suwannapoom C, Dahn HA, et al. 2020. A combined approach of mitochondrial DNA and anchored nuclear phylogenomics sheds light on unrecognized diversity, phylogeny, and historical biogeography of the torrent frogs, genus *Amolops* (Anura: Ranidae). *Molecular Phylogenetics and Evolution*, **148**: 106789.

Wu YK, Jiang K, Hanken J. 2010. A new species of newt of the genus *Paramesotriton* (Salamandridae) from southwestern Guangdong, China, with a new northern record of *P. longliensis* from western Hubei. *Zootaxa*, **2494**(1): 45−58.

Wu YK, Rovito SM, Papenfuss TJ, Hanken J. 2009. A new species of the genus *Paramesotriton* (Caudata: Salamandridae) from Guangxi Zhuang Autonomous Region, southern China. *Zootaxa*, **2060**(1): 59−68.

Xiang KL, Erst AS, Yang J, Peng HW, del C. Ortiz R, Jabbour F, et al. 2021. Biogeographic diversification of *Eranthis* (Ranunculaceae) reflects the geological history of the three great Asian plateaus. *Proceedings of the Royal Society B*, **288**(1948): 20210281.

Xiang XG, Mi XC, Zhou HL, Li JW, Chung SW, Li DZ, et al. 2016. Biogeographical diversification of mainland Asian *Dendrobium* (Orchidaceae) and its implications for the historical dynamics of evergreen broad-leaved forests. *Journal of Biogeography*, **43**(7): 1310−1323.

Xing YJ, Zhou LZ, Zhang YY, Wang XJ. 2008. Geographical patterns based on faunal types of breeding birds and mammals in China. *Integrative Zoology*, **3**(4): 280−289.

Xu W, Che J. 2019. From cryptic species to biodiversity conservation in China: status and prospects. *Scientia Sinica Vitae*, **49**(4): 519−530. (in Chinese)

Xu W, Dong WJ, Fu TT, Gao W, Lu CQ, Yan F, et al. 2021. Herpetological phylogeographic analyses support a Miocene focal point of Himalayan uplift and biological diversification. *National Science Review*, **8**(9): nwaa263.

Yan F, Nneji LM, Jin JQ, Yuan ZY, Chen JM, Mi X, et al. 2021. Multi-locus genetic analyses of *Quasipaa* from throughout its distribution. *Molecular Phylogenetics and Evolution*, **163**: 107218.

Yan Y, Yao D, Tian ZX, Huang CY, Dilek Y, Clift PD, et al. 2018. Tectonic topography changes in Cenozoic East Asia: a landscape erosion-sediment archive in the South China Sea. *Geochemistry, Geophysics, Geosystems*, **19**(6): 1731−1750.

Ye CY, Fei L. 2001. Phylogeny of genus *Odorrana* (Amphibia: Ranidae) in China. *Acta Zoologica Sinica*, **47**(5): 528−534. (in Chinese)

Yu Y, Harris AJ, Blair C, He XJ. 2015. RASP (Reconstruct Ancestral State in Phylogenies): a tool for historical biogeography. *Molecular Phylogenetics and Evolution*, **87**: 46−49.

Yuan ZY, Wu YK, Zhou JJ, Che J. 2016a. A new species of the genus *Paramesotriton* (Caudata: Salamandridae) from Fujian, southeastern China. *Zootaxa*, **4205**(6): 549−563.

Yuan ZY, Zhang BL, Raxworthy CJ, Weisrock DW, Hime PM, Jin JQ, et al. 2018. Natatanuran frogs used the Indian Plate to step-stone disperse and radiate across the Indian Ocean. *National Science Review*, **6**(1): 10−14.

Yuan ZY, Zhao HP, Jiang K, Hou M, He LZ, Murphy RW, et al. 2014. Phylogenetic relationships of the genus *Paramesotriton* (Caudata: Salamandridae) with the description of a new species from Qixiling nature reserve, Jiangxi, southeastern China and a key to the species. *Asian Herpetological Research*, **5**(2): 67−79.

Yuan ZY, Zhou WW, Chen X, Poyarkov Jr NA, Chen HM, Jang-Liaw NH, et al. 2016b. Spatiotemporal diversification of the true frogs (genus *Rana*): a historical framework for a widely studied group of model organisms. *Systematic Biology*, **65**(5): 824−842.

Zachos J, Pagani M, Sloan L, Thomas E, Billups K. 2001. Trends, rhythms, and aberrations in global climate 65 Ma to present. *Science*, **292**(5517): 686−693.

Zeng ZC, Liang D, Li JX, Lyu Z, Wang YY, Zhang P. 2020. Phylogenetic relationships of the Chinese torrent frogs (Ranidae: *Amolops*) revealed by phylogenomic analyses of AFLP-Capture data. *Molecular Phylogenetics and Evolution*, **146**: 106753.

Zhang D, Gao FL, Jakovlić I, Zou H, Zhang J, Li WX, et al. 2020. PhyloSuite: an integrated and scalable desktop platform for streamlined molecular sequence data management and evolutionary phylogenetics studies. *Molecular Ecology Resources*, **20**(1): 348−355.

Zhang P, Papenfuss TJ, Wake MH, Qu LH, Wake DB. 2008. Phylogeny and biogeography of the family Salamandridae (Amphibia: Caudata) inferred from complete mitochondrial genomes. *Molecular Phylogenetics and Evolution*, **49**(2): 586−597.

Zhang RZ. 2011. Zoogeography of China. Beijing: Science Press. (in Chinese)

Zhang YY, Li SQ. 2013. Ancient lineage, young troglobites: recent colonization of caves by *Nesticella* spiders. *BMC Evolutionary Biology*, **13**: 183.

Zhang ZG. 1980. Karst types in China. *Geojournal*, **4**(6): 541−570.

Zhao HT, Che J, Zhou WW, Chen YX, Zhao HP, Zhang YP. 2008. A new species of *Paramesotriton* (Caudata: Salamandridae) from Guizhou Province, China. *Zootaxa*, **1775**(1): 51−60.

Zhao HT, Hu SY, Wang YB, Chen YX. 2012. The biological characteristics and protection measures of *Paramesotriton zhijinensis*. *Sichuan Journal of Zoology*, **31**(5): 760–762, 850. (in Chinese)

Zhao JL, Paudel BR, Yu XQ, Zhang J, Li QJ. 2021. Speciation along the elevation gradient: Divergence of *Roscoea* species within the south slope of the Himalayas. *Molecular Phylogenetics and Evolution*, **164**: 107292.

Zhao JL, Xia YM, Cannon CH, Kress WJ, Li QJ. 2016. Evolutionary diversification of alpine ginger reflects the early uplift of the Himalayan–Tibetan Plateau and rapid extrusion of Indochina. *Gondwana Research*, **32**: 232−241.

Zhao YH, Zhang CG. 2009. Endemic Fishes of *Sinocyclocheilus* (Cypriniformes: Cyprinidae) in China: Species Diversity, Cave Adaptation, Systematics and Zoogeography. Beijing: Science Press. (in Chinese)

Zhao Z, Li SQ. 2017. Extinction vs. rapid radiation: the juxtaposed evolutionary histories of coelotine spiders support the Eocene–Oligocene orogenesis of the Tibetan Plateau. *Systematic Biology*, **66**(6): 988−1006.

Zheng HB. 2015. Birth of the Yangtze River: age and tectonic-geomorphic implications. *National Science Review*, **2**(4): 438−453.

Zheng HB, Clift PD, Wang P, Tada R, Jia JT, He MY, et al. 2013. Pre-miocene birth of the Yangtze River. *Proceedings of the National Academy of Sciences of the United States of America*, **110**(19): 7556−7561.

Zhou J, Wang SW, Xiao N, Luo T, Wang XL, Wang YL. 2021. Lineage diversification of the *Andrias davidianus* complex and classification evaluation of the Chinese giant salamander in Guizhou. *Journal of Guizhou Normal University:Natural Sciences*, **39**(2): 1−14. (in Chinese)

Zhou QY, Chen PY. 1993. Lithofacies change and palaeogeographical evolution during Late Cenozoic in Guizhou and its vicinity. *Geology of Guizhou*, **10**(3): 201−207. (in Chinese)

Zhou Y, Wang SR, Zhu HD, Li PP, Yang BT, Ma JZ. 2017. Phylogeny and biogeography of South Chinese brown frogs (Ranidae, Anura). *PLoS One*, **12**(4): e0175113.